Constitutively active RAS in *S. pombe* causes persistent Cdc42 signalling but only transient MAPK activation

Emma J. Kelsall[1,8], Ábel Vértesy[2,6,8], Kees Straatman[3], Mishal Tariq[1], Raquel Gadea[1,4], Chandni Parmar[1], Gabriele Schreiber[2], Shubhchintan Randhawa[1,7], Cyril Dominguez[1,5], Edda Klipp[2]* and Kayoko Tanaka[1,9]*

1 Department of Molecular and Cell Biology, University of Leicester

2 Theoretical Biophysics, Institute of Biology, Humboldt-Universität zu Berlin

3 Centre for Core Biotechnology Services, University of Leicester

4 Marco Formacion Profesional, Calle del Conde de Aranda 7-9, 50004 Zaragoza, Spain

5 Leicester Institute of Structural and Chemical Biology, University of Leicester

6 Present address: Hubrecht Institute-KNAW (Royal Netherlands Academy of Arts and Sciences) and University Medical Center, 3584 CT Utrecht, The Netherlands

7 Present address: Sanjay Gandhi Post Graduate Institute of Medical Sciences, Department of Molecular Medicine & Biotechnology, Lucknow, India 226014

8 These authors contributed equally

9 Lead Contact

*Correspondence: kt96@le.ac.uk (K.T.), edda.klipp@rz.hu-berlin.de (E.K.)

Highlights

(1) Constitutive Ras1.GV causes over-activation of Cdc42 in *S. pombe* pheromone signaling

(2) Ras1.GV induces an acute but only transient $MAPK^{Spk1}$ activation

(3) The RAS effector pathways $MAPK^{Spk1}$ and Cdc42 compete with each other for active Ras1

(4) Predictive modelling explains $MAPK^{Spk1}$ activation dynamics in 24 signaling-mutants

eTOC Blurb

S. pombe Ras1 activates the $MAPK^{Spk1}$ and Cdc42 pathways. Kelsall et al. report that the constitutively active Ras1.G17V mutation, which causes morphological anomalies, induces prolonged Cdc42 activation and $MAPK^{Spk1}$ activation followed by attenuation. Mathematical modelling shows competition between the $MAPK^{Spk1}$ and Cdc42 pathways for active Ras1.

Summary

The small GTPase RAS is a signalling hub. Oncogenic RAS mutations are assumed to over-activate all of the downstream pathways. We tested this assumption in fission yeast, where, RAS-mediated pheromone signalling (PS) activates the $MAPK^{Spk1}$ and Cdc42 pathways. Unexpectedly, we found that constitutively active Ras1.G17V induced acute transient $MAPK^{Spk1}$ activation, whilst Cdc42 activation persisted. Acute transient $MAPK^{Spk1}$ activation was also seen in the deletion mutant of Cdc42-GEF^{Scd1}, a Cdc42 activator. We have built a mathematical model using PS negative-feedback circuits and competition between the two Ras1 effectors, $MAPKKK^{Byr2}$ and Cdc42-GEF^{Scd1}. The model robustly predicted the $MAPK^{Spk1}$ activation dynamics of an additional 21 PS mutants. Supporting the model, we show that a recombinant Cdc42-GEF^{Scd1} fragment competes with $MAPKKK^{Byr2}$ for Ras1 binding. Our study has established a concept that constitutive RAS yields biased Cdc42/Rac over-activation, providing a strong rationale to interfere with this process to target oncogenic RAS in humans.

Key words

Ras, MAPK, Cdc42/Rac, yeast pheromone signalling

52 **Introduction**

53 Proto-oncogene Ras GTPase family members are widely conserved and play pivotal roles in cell
54 growth, differentiation and apoptosis (Cox and Der, 2010). The physiological impact of Ras
55 mutations is highlighted in the resultant tumorigenesis and developmental disorders (Prior et
56 al., 2012; Schubbert et al., 2007). More than 99% of identified oncogenic RAS mutations occur at
57 codons 12, 13 and 61 of human Ras isoforms (Prior et al., 2012) and impair efficient GTP
58 hydrolysis (Trahey and McCormick, 1987). This results in accumulation of GTP-bound Ras, which
59 is generally considered to cause constitutive activation of the downstream effector pathways,
60 such as ERK and PI3K signalling pathways (Lin et al., 1998; Zhu et al., 1998). Interestingly, mouse
61 embryonic fibroblasts (MEFs) derived from the *K-ras*^{G12D} mouse model show neither an
62 increased basal level of active ERK and Akt nor constitutive activation of ERK and Akt upon
63 growth factor stimulation even though the *K-ras*^{G12D} MEFs showed enhanced proliferation and
64 partial transformation (Tuveson et al., 2004). This observation indicates that not all effector
65 pathways become constitutively activated by oncogenic Ras, presumably because of an efficient
66 negative feedback loop. Meanwhile, it is reasonable to expect that oncogenic RAS over-activates
67 some of its effector pathways to initiate tumorigenesis. Small GTPases, including Cdc42 and Rac,
68 may be such effector pathways, as they are required in oncogenic-RAS-driven tumorigenesis
69 (Malliri et al., 2002; Qiu et al., 1997; Stengel and Zheng, 2012).

70 We wished to understand how multiple Ras effector pathways respond to the Ras-triggered
71 signals in a physiological setting. We employed the model organism fission yeast. In this
72 organism, a unique Ras homologue, Ras1, plays a key role in pheromone signalling to cause
73 mating of haploid cells and sporulation in diploid cells (Yamamoto, 1996)(Fig. 1A, B). Upon
74 nutritional starvation, cells of opposite mating types (h^+ and h^-) exchange mating pheromones.
75 Gpa1, the α-subunit of the pheromone receptor-coupled G-protein, relays the pheromone
76 signal into the cell (Obara et al., 1991). Activated Gpa1 together with Ras1 then activate MAPK
77 cascade consisting of Byr2 (MAPKKK), Byr1 (MAPKK) and Spk1 (MAPK) (Fukui et al., 1986;
78 Masuda et al., 1995; Nadin-Davis and Nasim, 1988; Nadin-Davis et al., 1986a; Nadin-Davis et al.,
79 1986b; Wang et al., 1991; Xu et al., 1994). An intriguing observation is that the *ras1.G17V*
80 mutant, an equivalent of mammalian *ras.G12V* mutant prevalent in cancer, produces an
81 excessively elongated shmoo, or a conjugation tube, upon exposure to the mating pheromone
82 (Nadin-Davis et al., 1986a). This "elongated" *ras1.G17V* phenotype has been interpretted that

83 Ras1 might be directly responsible for amplifying the pheromone signal at an intracellular level
84 (Yamamoto, 1996).
85 Ras1 also regulates cell morphology during vegetative growth; whilst deletion of either *gpa1*,
86 *MAPKKK*^{byr2}, *MAPKK*^{byr1} or *MAPK*^{spk1} does not result in any obvious phenotypes during vegetative
87 cell growth (Obara et al., 1991; Sipiczki, 1988; Toda et al., 1991), *ras1Δ* cells lose the typical rod-
88 shape morphology of fission yeast to become rounded (Fukui et al., 1989; Nadin-Davis et al.,
89 1986a). Studies based on recombinant protein assays and yeast-2-hybrid analysis demonstrated
90 that Ras1 interacts with both MAPKKK^{Byr2} and Scd1, a GDP-GTP exchange factor (GEF) for Cdc42,
91 which regulates the actin cytoskeleton and cell morphology (Chang et al., 1994; Gronwald et al.,
92 2001; Tu et al., 1997). These observations suggest that Ras1 simultaneously regulates both the
93 pheromone MAPK^{Spk1} and the Cdc42 pathways at the cell membrane (Weston et al., 2013).
94 Indeed, a dynamic "Cdc42 zone" at the cell cortex prior to mating has been observed (Merlini et
95 al., 2013) and Ras1 and MAPK^{Spk1} cascade components are found there and are involved in the
96 process (Dudin et al., 2016; Merlini et al., 2013; Merlini et al., 2016; Merlini et al., 2018; Weston
97 et al., 2013). However, it is not yet understood how Ras1 interplay between the two pathways.
98 By establishing conditions to induce highly synchronous mating of fission yeast cells, for the first
99 time we were able to follow MAPK^{Spk1} activation during the physiological mating process in
100 wildtype and in mutants showing various mating phenotypes. This comprehensive set of
101 quantitative measurements allowed us to build a mathematical model of the Ras-mediated
102 pheromone signalling. Our model can serve as a prototype of a branched Ras-mediated
103 signalling pathway, demonstrating a competition of downstream pathways for a common
104 upstream activator, Ras1. The model also highlights the physiological importance of the
105 bipartite activation of MAPKKK^{Byr2}: a Ras1-dependent and a Ras1-independent mechanism, the
106 latter of which employs the adaptor protein Ste4 (Barr et al., 1996; Okazaki et al., 1991). The
107 adaptor^{Ste4} can be targeted to downregulate MAPK^{Spk1} even in the presence of *ras1.G17V*
108 mutation. Finally, our study reveals the crucial role played by Cdc42 in the *ras1.G17V* mutant
109 causing the *ras1.G17V* phenotype.
110

111 **Results**

112

113 **(1) A highly synchronous mating assay allows the precise measurement of MAPK^{Spk1} activity**

114 To directly measure fission yeast pheromone signalling, we quantitated MAPK^{Spk1}
115 phosphorylation throughout the mating process (Fig. S1, Fig. 1A and B). We established a
116 protocol to induce highly synchronous mating and employed cells where the endogenous
117 MAPK^{Spk1} is tagged with GFP-2xFLAG. Under these conditions, homothallic *h^{90}* cells started to
118 mate 7-hours after induction of mating (Fig. 1C, grey line). Phosphorylated (active) MAPK^{Spk1}
119 (**pp**MAPK^{Spk1}) levels were quantitated as described in Materials and Methods.
120 The **pp**MAPK^{Spk1} signal was first detected three hours after induction of mating and reached its
121 peak at about seven hours, when cell fusion was also initially observed (Fig. 1C, blue line). The
122 **pp**MAPK^{Spk1} then gradually decreased to a non-zero level as meiosis continued towards
123 sporulation. The observation established that the MAPK^{Spk1}-GFP activation occurs as the mating
124 process progresses and declines before sporulation, around 15 hours post induction. It was also
125 noted that the total MAPK^{Spk1}-GFP was essentially not expressed during the vegetative cycle,
126 but it was promptly induced by nitrogen starvation (Supplementary Fig. S2A and S2B). The
127 *mapk^{spk1}* gene is a known target of the transcription factor Ste11 (Mata and Bahler, 2006),
128 which itself is activated (phosphorylated) by MAPK^{Spk1} (Kjaerulff et al., 2005). This positive
129 feedback loop likely facilitates a swift increase of MAPK^{Spk1} expression upon nitrogen starvation.
130 We found that MAPK^{Spk1}-GFP localised to both the cytosol and the nucleus, with some nuclear
131 accumulation, before it gradually disappeared as the mating process came to the end (Fig. 1D).
132 Interestingly, transient foci of GFP signals were also found at the cell cortex, as has been
133 reported for MAPKK^{Byr1}, the activator of MAPK^{Spk1} (Dudin et al., 2016) (Fig. 1D, yellow arrows).

134

135 **(2) Constitutively active MAPKK$^{Byr1.DD}$ mutant causes constitutive activation of MAPK^{Spk1}**

136 Activation of MAPKK family kinases is mediated by dual phosphorylation of conserved Ser/Thr
137 residues (Zheng and Guan, 1994). These correspond to serine 214 and threonine 218 of the
138 MAPKK^{Byr1}. A MAPKK^{Byr1} mutant termed MAPKK$^{Byr1.DD}$, which carries aspartic acid substitution at
139 these sites, was expected to act as a constitutively active MAPKK (Ozoe et al., 2002). We
140 introduced the *MAPKK$^{byr1.DD}$* mutation at its chromosome locus and measured the activation
141 profile of its target, MAPK^{Spk1} during the mating process. The increase of the **pp**MAPK^{Spk1} signal
142 in the *MAPKK$^{byr1.DD}$* mutant strain was delayed compared to the wildtype strain and the

143 **pp**MAPK^{Spk1} accumulated at a slower rate (Fig. 1E, light green line). However, the level of
144 **pp**MAPK^{Spk1} remained high after reaching its highest intensity at around 16 hours after
145 induction, resulting in a constitutive phosphorylation of MAPK^{Spk1} (Fig. 1E and Supplementary
146 Fig. S2C and S2D). This result highlights that the suggested de-phosphorylation of **pp**MAPK^{Spk1}
147 by phosphatases Pmp1 and Pyp1 (Didmon et al., 2002) is not efficient in downregulating the
148 pheromone signalling in the presence of MAPKK$^{Byr1.DD}$. The MAPKK$^{Byr1.DD}$ strain is also less
149 competent in finding the partner mating cell than cells with wildtype MAPKK^{Byr1}. We also
150 confirmed the intriguing *"fus"* (fusion deficient) phenotype of cells expressing MAPKK$^{Byr1.DD}$ from
151 its native promoter (Fig.1F) (Dudin et al., 2016; Ozoe et al., 2002). These cells find their partners
152 and pair up successfully but fail to fuse with each other, resulting in *fus* phenotype. Consistent
153 with the observed slower increase in **pp**MAPK^{Spk1} (Fig.1E) the nuclear localisation of MAPK^{Spk1}
154 was also delayed compared to Wildtype cells (Fig 1F). A strong MAPK^{Spk1}-GFP signal was then
155 observed in the nuclei of the paired *fus* cells and the nuclear MAPK^{Spk1}-GFP signal persists even
156 24 hours after the induction of mating (Fig. 1F). Interestingly, the projection tips of the paring
157 cells often show increased MAPK^{Spk1}-GFP signal (Fig. 1F, yellow arrows). These results conclude
158 that MAPK^{Spk1} activation is highly influenced by the MAPKK^{Byr1} status and phosphatases directly
159 regulating MAPK^{Spk1} cannot counteract MAPKK$^{Byr1.DD}$.
160
161 **(3) The *ras1.G17V* mutation causes acute transient MAPK^{Spk1} activation**
162 The fission yeast equivalent of human oncogenic *ras.G12V* is *ras1.G17V,* which induces an
163 excessively elongated shmoo, and the cells fail to recognize a partner and become sterile (Fukui
164 et al., 1986; Nadin-Davis et al., 1986a). The "elongated shmoo" phenotype was interpreted as
165 an excess activation of the downstream pathway(s) of Ras1, leading to a prediction that the
166 *ras1.G17V* causes over-activation of MAPK^{Spk1} (Weston et al., 2013; Yamamoto, 1996). However,
167 no direct evidence has been provided.
168 Quantitation of the **pp**MAPK^{Spk1}-GFP in the *ras1.G17V* mutant showed an acute increase of the
169 **pp**MAPK^{Spk1}-GFP upon induction of mating (Fig. 1G, Green line). However, the signal intensity
170 declined gradually and by 16 hours after induction the level was comparable to wildtype cells,
171 indicating that down-regulation of **pp**MAPK$^{Spk1\text{-}GFP}$ is effective, unlike in *MAPKK$^{byr1.DD}$* mutant.
172 Correspondingly, the cellular MAPK^{Spk1}-GFP signal also declined 24 hours after induction of
173 mating (Fig. 1H). Collectively, these observations indicate that the down-regulation mechanism
174 for **pp**MAPK^{Spk1} is robust and resistant to Ras1.G17V. It was also noted that the peak intensity of

175 the **pp**MAPK^{Spk1} was somewhat lower and the rate of signal reduction was slightly decreased
176 compared to wildtype cells (Fig. 1G).
177
178 **(4) The elongated *ras1.G17V* shmoos develop with a minimum level of MAPK^{Spk1}: neither**
179 **amplitude nor duration of ppMAPK^{Spk1} signal influences the *ras1.G17V* phenotype**
180 Having observed that *MAPKK$^{byr1.DD}$* and *ras1.G17V* show different MAPK^{Spk1} activation profiles
181 (sustained vs transient) and different morphological phenotypes ("*fus*" vs elongated), we
182 examined a link between the MAPK^{Spk1} activation profiles and the cell morphology. The
183 MAPK^{Spk1} phosphorylation profile of the cells harbouring both *ras1.G17V* and *MAPKK$^{byr1.DD}$*
184 mutations (*ras1.G17V MAPKK$^{byr1.DD}$* double mutant) was comparable to the cells harbouring
185 *MAPKK$^{byr1.DD}$* mutation only; it showed a slow increase of the **pp**MAPK^{Spk1}-GFP level, which
186 reached the plateau at about 16 hours after induction of mating (Fig. 2A, red line). The nuclear
187 **pp**MAPK^{Spk1}-GFP signal in the *ras1.G17V MAPKK$^{byr1.DD}$* double mutant was also present 24 hours
188 after induction of mating, unlike the *ras1.G17V* single mutant cells, confirming that the
189 *ras1.G17V MAPKK$^{byr1.DD}$* double mutant cells retained a high **pp**MAPK^{Spk1} level. Thus, in terms of
190 the activation status of MAPK^{Spk1}, *MAPKK$^{byr1.DD}$* is epistatic to *ras1.G17V*.
191 In terms of cell morphology, the *ras1.G17V MAPKK$^{byr1.DD}$* double mutant cells showed the
192 "elongated" *ras1.G17V* phenotype (Fig. 2B), but not the "paired" *MAPKK$^{byr1.DD}$* phenotype.
193 Therefore, *ras1.G17V* was epistatic to *MAPKK$^{byr1.DD}$* in terms of the elongated shmoo
194 morphology.
195 Interestingly, obvious shmoo formation in the *ras1.G17V MAPKK$^{byr1.DD}$* double mutant was first
196 noticed 16 hours after induction of mating, much later than the *ras1.G17V* single mutant, but as
197 a similar timing as the *MAPKK$^{byr1.DD}$* single mutant (Fig. 2B). Given the slow increase of the
198 **pp**MAPK^{Spk1} signal in mutants harbouring the *MAPKK$^{byr1.DD}$* mutation, we predicted that the
199 delayed appearance of the *ras1.G17V* shmoo meant that the *ras1.G17V* shmoo formation still
200 requires a certain level of MAPK^{Spk1} activity. Indeed, when *MAPKK^{byr1}* was deleted in the
201 *ras1.G17V* mutant, not only was the MAPK^{Spk1} activation and nuclear MAPK^{Spk1}-GFP signal
202 abolished (Fig. S1F), but also shmoo formation was abrogated as in the *MAPKK$^{byr1}\Delta$* single
203 mutant (Fig. 2C). Based on these observations, we concluded that the cell morphology is
204 determined by the molecular status of Ras1, and not by the MAPK^{Spk1} activation profile. Yet, the
205 *ras1.G17V* phenotype still requires MAPK^{Spk1} activity, which determines the timing of shmoo
206 formation.

207

208 **(5) Cdc42 is required for the shmoo formation but not for the MAPK^{Spk1} activation**

209 During the vegetative cycle, *ras1Δ* cells show spherical cell morphology (Fukui et al., 1986;
210 Nadin-Davis et al., 1986a) and polarised localisation of active Cdc42 is compromised (Kelly and
211 Nurse, 2011), (Fig. 4C, D), indicating that Ras1 is involved in Cdc42 activation. The GTP-loaded
212 Cdc42 is then predicted to activate the downstream Ste20-like kinase, Pak1/Shk1 (Endo et al.,
213 2003; Marcus et al., 1995; Ottilie et al., 1995; Verde et al., 1995), resulting in actin
214 reorganisation and shmoo formation under mating conditions (Bendezu and Martin, 2013;
215 Merlini et al., 2016).

216 To confirm that Cdc42 acts downstream of Ras1, we generated a double mutant strain
217 harbouring *ras1.G17V* and deletion of *scd1*, encoding a GDP-GTP exchanging factor for Cdc42
218 (Cdc42-GEF^{Scd1}). The *ras1.G17V* elongated shmoo phenotype was lost in the double mutant and
219 instead, the cells showed a mating-deficient phenotype similar to the *cdc42-GEF^{scd1}Δ* single
220 mutant (Fig 3A). The result supports the model that Cdc42 acts downstream of Ras1 to cause
221 morphological changes.

222 Intriguingly, in the strains harbouring the *cdc42-GEF^{scd1}Δ* mutation, a nuclear MAPK^{Spk1}-GFP
223 signal appeared (Fig. 3A), indicating that activation of MAPK^{Spk1} may not be impaired by lack of
224 active Cdc42. This was unexpected because in a previous study, it was predicted that activation
225 of Cdc42 contributes to activation of MAPKKK^{Byr2} (Tu et al., 1997). To clarify this issue, we
226 measured **pp**MAPK^{Spk1} in the *cdc42-GEF^{scd1}Δ* mutant. Strikingly, in these cells MAPK^{Spk1}
227 activation occurred with a reproducible advancement of the initial activation timing compared
228 to the wildtype cells (Fig. 3B). The result shows that MAPK^{Spk1} activation does not require Cdc42
229 activity. Additionally, the faster activation of MAPK^{Spk1} raises the interesting possibility that two
230 Ras1 effectors, MAPKKK^{Byr2} and Cdc42-GEF^{Scd1}, are competing with each other for activated
231 Ras1, thus, lack of Cdc42-GEF^{Scd1} results in an advanced MAPK^{Spk1} activation (modelled in Fig.
232 7A).

233 Substantial MAPK^{Spk1} activation in the *cdc42-GEF^{scd1}Δ* mutant means that the mating deficiency
234 of this mutant is unlikely to be the result of the lack of MAPK^{Spk1} activation. Indeed, introduction
235 of *MAPKK$^{byr1.DD}$* to the *cdc42-GEF^{scd1}Δ* mutant did not restore the mating deficient phenotype,
236 even though nuclear MAPK^{Spk1}-GFP highly accumulated (Fig. 3C). The result shows that active
237 Cdc42 function is absolutely required for the mating process regardless of the MAPK^{Spk1}

238 activation status. Taken together with the essential role of MAPK^{Spk1}, we concluded that the
239 mating pheromone signalling feeds into at least two pathways, MAPK^{Spk1} and Cdc42.
240
241 **(6) Ras1 activates two effector pathways, MAPK^{Spk1} and Cdc42.**
242 In order to further clarify the role of Ras1 we examined the MAPK^{Spk1} activation status and cell
243 morphology in the following four strains: *ras1Δ* mutant, *ras1Δ MAPKK$^{byr1.DD}$* double mutant,
244 *MAPKKK^{byr2}Δ* mutant and *MAPKKK^{byr2}Δ MAPKK$^{byr1.DD}$* double mutant. As mentioned earlier,
245 deletion of *ras1* causes cells to show a round morphology (Fig. 3F), with reduced cortical signal
246 of CRIB-GFP, an indicator of the active GTP-bound form of Cdc42, showing that Cdc42 activation
247 is compromised (Fig.4C, D). *ras1* deletion also causes substantial reduction, but not complete
248 elimination, of the **pp**MAPK^{Spk1} (Fig. 3D, red line, and Supplementary Fig. S3A); thus, Ras1 plays
249 an important role in activating both Cdc42 and MAPK^{Spk1} pathways. Introduction of the
250 *MAPKK$^{byr1.DD}$* mutation into the *ras1Δ* mutant cells induces the constitutive **pp**MAPK^{Spk1} (Fig. 3D,
251 green line and Supplementary Fig. S3A) but does not affect the round cell morphology and cells
252 remain sterile (Fig. 3F, the 2nd left panel. Note the accumulating MAPK^{Spk1}-GFP at 16 hours after
253 induction of mating), as was the case for the *Cdc42-GEF^{Scd1}Δ MAPKK$^{byr1.DD}$* double mutant (Fig.
254 3C).
255 In a striking contrast, the sterile phenotype of the *MAPKKK^{byr2}Δ*, associated with complete lack
256 of shmoo formation (Fig. 3F, the 2nd right panel), was converted to the "*fus*" phenotype, when
257 combined with the *MAPKK$^{byr1.DD}$* mutation (Fig. 3F, the far right panel). As expected, the
258 *MAPKKK^{byr2}Δ MAPKK$^{byr1.DD}$* double mutant shows MAPK^{Spk1} constitutive activation (Fig. 3E and
259 Supplementary Fig. S3B). Thus, unlike the cases of *scd1Δ* or *ras1*Δ, lack of *MAPKKK^{byr2}* can be
260 bypassed by constitutive activation of MAPK^{Spk1}, indicating that the sole role of MAPKKK^{Byr2} is to
261 activate the MAPK^{Spk1} unlike its upstream activator, Ras1, which also activates Cdc42 pathway (a
262 model presented in Fig. 7A).
263
264 **(7) Ras1.G17V causes accumulation of Cdc42-GTP at the cell cortex.**
265 Having observed a relatively mild influence of Ras1.G17V towards the MAPK^{Spk1} activation, we
266 next examined whether the Cdc42 pathway was affected by the *ras1.G17V* mutation. We
267 visualized the active GTP-bound form of Cdc42 (Cdc42^{GTP}) using CRIB-GFP that specifically binds
268 to Cdc42^{GTP} (Tatebe et al., 2008). As previously observed, dynamic foci of CRIB-GFP appeared on
269 the cell cortex upon induction of mating (Bendezu and Martin, 2013)(Fig. 4A and B). In our

experimental condition, more than 80% of wildtype cells showed the cortical CRIB-GFP signal at 4.5 hours after induction of mating (Fig. 4B). The cortical CRIB-GFP foci became concentrated at the site of mating and quickly disappeared once cells fused successfully to form zygotes (Fig. 4A and B). In striking contrast, in the *ras1.G17V* mutant cells, the cortical CRIB-GFP signal persisted, often at the elongated tip end of the cells, even 12.5 hours after induction of mating (Fig. 4A and B). The signal could still be seen in about 40% of the cells 22.5 hours after induction of mating (Fig. 4A and B). The result shows that the Cdc42 pathway is excessively activated in the *ras1.G17V* mutant and the localisation pattern of $Cdc42^{GTP}$ indicates that the signature "elongated" *ras1.G17V* morphological phenotype is caused by deregulation of the Cdc42 pathway.

Ras1-mediated Cdc42 pathway activation has been also indicated during the vegetative growth where the *ras1Δ* mutant shows a round cell morphology (Chang et al., 1994; Kelly and Nurse, 2011). However, unlike during the mating process, the *ras1.G17V* mutation does not cause an obvious morphological phenotype during the vegetative growth. We predicted that, during the vegetative growth, rigorous negative regulation occurs for Cdc42 by GTPase activation protein(s) (GAPs), such as Rga4 (Das et al., 2007; Kelly and Nurse, 2011; Tatebe et al., 2008) to counteract the effect of *ras1.G17V*. To examine this possibility, we compared Cdc42 activation status of vegetatively growing wildtype, *ras1*Δ, *ras1.G17V*, *rga4Δ*, and *rga4Δ ras1.G17V* double mutant cells (Fig. 4C and D). As previously described, CRIB-GFP showed a clearly polarized signal at the growing cell tips in the wildtype strain (Tatebe et al., 2008)(Fig. 4C and D). In the *ras1*Δ mutant, the cells were round and CRIB-GFP signal on the cell cortex had largely disappeared as was seen in the *cdc42-GEF*^{scd1}Δ mutant (Kelly and Nurse, 2011). In contrast, the cortical CRIB-GFP signal was clearly increased in the *ras1.G17V* single mutant although the cell morphology appeared largely similar to the wildtype cells (Fig. 4C, D). These results indicate a direct involvement of Ras1 in activating Cdc42. Meanwhile, the *rga4Δ* mutant cells showed slight alterations to the cell morphology, accompanied with less polarized distribution of cortical CRIB-GFP signal, as has been reported (Fig. 4C and D) (Das et al., 2007; Kelly and Nurse, 2011; Tatebe et al., 2008). Strikingly, the *rga4Δ ras1.G17V* double mutant showed a clear morphological alteration (big round cells) and the strongest cortical CRIB-GFP signal among all the mutants examined (Fig. 4C and D). The result fits well with our hypothesis that Ras1.G17V is activating Cdc42 even during vegetative growth, but the overall effect of Ras1.G17V is counteracted by the Cdc42-GAP, Rga4.

303 **(8) Ras1 and an adaptor protein Ste4 are both necessary to fully activate MAPKKK^{Byr2}**
304
305 Although Ras1 clearly plays the major role to activate MAPK^{Spk1}, a marginal, but detectable level
306 of **pp**MAPK^{Spk1} was still induced in the *ras1Δ* mutant (Fig. 3D and Supplementary Fig. S3A),
307 indicating that there is a Ras1-independent mechanism to activate MAPK^{Spk1}. Previous studies
308 proposed an adaptor protein, Ste4, to be involved in the activation of MAPKKK^{Byr2}(Barr et al.,
309 1996; Okazaki et al., 1991; Ramachander et al., 2002; Tu et al., 1997). We therefore examined
310 whether Ste4 is required for MAPK^{Spk1} activation.
311 In constrast to the *ras1Δ* mutant, we detected virtually no MAPK^{Spk1} phosphorylation in the
312 *ste4Δ* mutant (Fig. 5A and Supplementary Figure S3C), indicating that the adaptor^{Ste4} is a
313 prerequisite for the MAPK^{Spk1} activation and the **pp**MAPK^{Spk1} signal observed in the *ras1Δ*
314 mutant is dependent on Ste4 function. Introduction of *ras1.G17V* mutation neither restored the
315 MAPK^{Spk1} activation nor mating (Fig. 5A, B), thus, activation of Ras1 cannot take over Ste4
316 function. In a striking contrast, the *ste4Δ MAPKK$^{byr1.DD}$* double mutant showed the *"fus"*
317 phenotype as the *MAPKK$^{byr1.DD}$* single mutant cells and induced constitutive MAPK^{Spk1} activation,
318 indicating that Ste4 is solely required for MAPK^{Spk1} activation (Fig. 5A, B).
319 Taken together, MAPKKK^{Byr2} is activated through a mechanism involving both Ras1 and Ste4, but
320 Ste4 only conveys the signal towards the MAPK^{Spk1}, while Ras1 also activates Cdc42.
321
322 **(9) Ste6, a Ras1 GTP-GDP exchange factor, contributes to both the MAPK^{Spk1} and the Cdc42**
323 **pathway activation**
324 There are two GDP-GTP exchange factors (GEFs) identified for Ras1: Ste6 and Efc25 (Hughes et
325 al., 1990; Tratner et al., 1997). As to the functional differences, Ste6 is essential for mating but is
326 dispensable during the vegetative cycle whilst Efc25 is dispensable for mating but is required to
327 maintain the cell morphology during the vegetative growth (Hughes et al., 1990; Tratner et al.,
328 1997). There has been an interesting proposition that Ste6 may specifically help Ras1 to activate
329 the MAPK^{Spk1} pathway, but not the Cdc42 pathway, whilst Efc25 specifically facilitates Ras1 to
330 activate the Cdc42 pathway (Papadaki et al., 2002). We examined this hypothesis by monitoring
331 the MAPK^{Spk1} activation status and conducting genetic epistasis analysis of *ras1.G17V* and
332 *MAPKK$^{byr1.DD}$* in the *ste6Δ* mutant.
333 In *ste6Δ* cells, MAPK^{Spk1} phosphorylation was found somewhat reduced but occurred at a clearly
334 detectable level. The signal increased when the *ras1.G17V* mutation was introduced (Fig. 5C and

335 Supplementary Figure S3D). When *ste6Δ and MAPKK*$^{byr1.DD}$ were combined, MAPK^{Spk1} signalling
336 recapitulated the *MAPKK*$^{byr1.DD}$ activation profile (Fig. 5C and Supplementary Figure S3D).
337 Nonetheless, the "pheromone-insensitive sterile" morphology of *ste6Δ* was only rescued by
338 *ras1.G17V*, as previously reported, exhibiting the "elongated" phenotype (Hughes et al., 1990),
339 but not by MAPKK$^{byr1.DD}$ (Fig. 5D). The result indicates that, unlike *ste4Δ* mutant, the mating
340 deficiency of *ste6Δ* is not caused by mere lack of MAPK^{Spk1} activation but by lack of Ras1
341 activation. We concluded that Ste6 functions to activate Ras1, which then activates *both* the
342 MAPK and Cdc42 pathways in response to pheromone signalling.
343
344 **(10) Activation mutant of Gpa1 mimics the full pheromone signalling**
345 In order to generate an integrated prototype Ras signalling model, we further investigated the
346 upstream signal input machinery. Previous studies showed that Gpa1 plays the primary role in
347 pheromone signalling (Obara et al., 1991). In agreement, in the *gpa1Δ* mutant we detected no
348 MAPK^{Spk1} activation nor nuclear accumulation of MAPK^{Spk1}-GFP (Fig. 6A, B and Supplementary
349 Fig. S4A). Introducing the *ras1.G17V* to the *gpa1Δ* strain did not rescue the complete lack of
350 *MAPK*^{Spk1} activation nor did it induce a shmoo-like morphological change (Fig. 6A, B and
351 Supplementary Fig. S4A), supporting our earlier observation that a Ras1-independent
352 mechanism, involving Ste4 is essential for MAPK^{Spk1} activation. Meanwhile, introducing the
353 *MAPKK*$^{byr1.DD}$ mutation caused the constitutive activation of MAPK^{Spk1} (Fig. 6A and
354 Supplementary Fig. S4A), but cells showed no morphological change (Fig. 6B). When both
355 *ras1.G17V* and *MAPKK*$^{byr1.DD}$ mutations were introduced into the *gpa1Δ* strain, MAPK^{Spk1} was
356 activated and a shmoo-like morphological change occurred (Fig. 6A, B and Supplementary Fig.
357 S4A). Therefore, activation of both of these two molecules is required and sufficient to mimic
358 the pheromone signalling.
359 To further confirm that the Gpa1 is a central component of pheromone signalling, we looked
360 into the MAPK^{Spk1} activation status in the constitutively active *gpa1.QL* mutant, which exhibits a
361 "shmoo-like" morphological change in the heterothallic *h*$^{-}$ strain without the mating partner
362 (Obara et al., 1991).
363 Upon nitrogen starvation, the *h*$^{-}$ *gpa1.QL* mutant strain showed morphological changes and a
364 strong MAPK^{Spk1} activation (Fig. 6C red line, Fig. 6D and Supplementary Fig. S4B). This response
365 was largely dependent on the Ras1 function as the *h*$^{-}$ *gpa1.QL ras1Δ* double mutant exhibited a
366 significantly reduced level of **pp**MAPK^{Spk1} and a round cell morphology, two typical features of

367 *ras1Δ* cells (Fig. 6C, D and Supplementary Fig. S4B). On the other hand, the *h⁻ ras1.G17V* single
368 mutant showed a very low level of $MAPK^{Spk1}$ activation, comparable to the one observed in the
369 *h⁻* wildtype strain, with no apparent morphological alternation, confirming that sole activation
370 of Ras1 does not substitute the pheromone signalling.
371 The *h⁻ MAPKK*$^{byr1.DD}$ mutant induced a strong constitutive $MAPK^{Spk1}$ activation, confirming that
372 the $MAPKK^{Byr1.DD}$ molecule can activate $MAPK^{Spk1}$ regardless of the pheromone signal input (Fig.
373 6C, light-blue line and Supplementary Fig. S4B). However, cell morphology was unchanged (Fig.
374 6D). Collectively, these results support the model where Gpa1 acts as the central transducer of
375 the pheromone signalling, which can be mimicked only if both $MAPK^{Spk1}$ and Ras1 are activated.
376
377 **(11) A holistic modelling framwork of $MAPK^{Spk1}$ activation**
378 Based on quantitative **pp**$MAPK^{Spk1}$ measurements in wildtype and various mutant strains (Fig.
379 1C, E, G, and Fig. 3B), we constructed a mathematical model of the $MAPK^{Spk1}$ signalling
380 dynamics. The aim of the model is to test whether a simple competition of the MAPK and the
381 Cdc42 pathways for a shared pool of active Ras^{GTP}, can explain why the *scd1Δ* strain shows the
382 similar **pp**$MAPK^{Spk1}$ activation profile as the *ras1.G17V* strain.
383 We designed a reductionist model of 6 ordinary differential equations to represent key steps of
384 pheromone signalling (Fig. 7A, Supplementary Fig. S5 and materials and methods). Model
385 simulations and parameter estimations were performed in COPASI (Hoops et al., 2006) and
386 details of the modelling process are described in Materials and Methods. Each biochemical
387 process is referred as [L1]-[L10] as depicted in Fig. 7A. The signalling components were set to
388 interact without delay based on the observations that signalling components are localized in
389 close proximity (Fig. 1 and Fig. 4)(Dudin et al., 2016; Merlini et al., 2016; Merlini et al., 2018).
390 The framework of the modelling process is as follows: Genes encoding pheromones, receptors,
391 Gpa1, Ste4 and Ste6 are all known to be under regulation of Ste11, the master transcriptional
392 regulator for meiotic genes (Hughes et al., 1994; Mata and Bahler, 2006; Mata et al., 2002; Mata
393 et al., 2007; Sugimoto et al., 1991) and these components are grouped into the Pheromone
394 Sensing (PS) unit. During the vegetative growth, the PS unit is set to zero. Nitrogen starvation
395 activates Ste11 (Kjaerulff et al., 2007; Sugimoto et al., 1991), which induces the PS unit [L1]. The
396 PS unit activates $MAPKKK^{Byr2}$ in a twofold manner: Directly by Ste4 [L3] and through Ras1
397 [L4](Fig. 7A). Activated $MAPKKK^{Byr2}$ then triggers activation of $MAPKK^{Byr1}$ [L5] that activates

398 MAPK^{Spk1} [L6]. Since activated MAPK^{Spk1} further activates Ste11 (Kjaerulff et al., 2005), MAPK^{Spk1}
399 has a positive feedback loop on its own expression via Ste11 [L2,L7] (Fig. 7A).
400 As the pheromone signalling was found to induce a transient **pp**MAPK^{Spk1} peak (Fig. 1C),
401 **pp**MAPK^{Spk1} activity is ought to be regulated by a delayed downregulation. Because the
402 *MAPKK$^{byr1.DD}$* mutant completely lacks downregulation (Fig. 1E), downregulation occurring
403 downstream of MAPKK^{byr1} (e.g.: Pyp1 and Pmp1) were considered physiologically insignificant.
404 Meanwhile, Sxa2 (a serine carboxypeptidase against a mating pheromone P-factor) and Rgs1 (a
405 regulator of Gpa1), both of which are induced upon successful pheromone signalling (Imai and
406 Yamamoto, 1992; Mata and Bahler, 2006; Pereira and Jones, 2001; Watson et al., 1999),
407 receptor internalization (Hirota et al., 2001) and regulation of the *mapk^{spk1}* transcript or other
408 components by antisense RNA (Bitton et al., 2011) fit well to the criteria for the negative
409 feedback. We represented all these potential negative feedbacks collectively as a single circuit,
410 [L8]. Importantly, this downregulation [L8] works unperturbed in the presence of Ras1.G17V, by
411 acting through the Ste4-dependent MAPKKK^{Byr2} activation process (Fig. 1G, Fig. 7A).
412 Ras1-GTP activates both the MAPKKK^{Byr2} and the Cdc42 pathways [L9] (Chang et al., 1994). As
413 opposed to previous expectations that active Cdc42^{GTP} is required to activate MAPKKK^{Byr2} (Tu et
414 al., 1997), deletion of Cdc42-GEF^{Scd1} does not compromise MAPK^{Spk1} activation (Fig. 3B) and
415 rather, it makes **pp**MAPK^{Spk1} dynamics remarkably similar to that of the Ras1.G17V strain (Fig.
416 3B and Fig. 1G, plotted together in Fig. 7B): in both cases, **pp**MAPK^{Spk1} peaks earlier than the
417 wildtype case. At a molecular level, reactions depleting the Ras1^{GTP} pool are compromised in
418 both strains. Therefore, to explain these observations, we hypothesized that MAPK^{Spk1} and
419 Cdc42 pathways are competing for the common Ras1^{GTP} pool. In this manner, one of the
420 pathways can modulate the other by changing the amount of unbound (available) Ras1^{GTP}.
421 In support of this prediction, we showed that binding of recombinant Ras1.G17V^{GTP} to a
422 MAPKKK^{Byr2} fragment was reduced by the presence of a Cdc42-GEF^{Scd1} fragment *in vitro* (Fig. 7C,
423 D). In this assay, bacterially expressed GST tagged fragments of both MAPKKK^{Byr2} (65-180) and
424 Cdc42-GEF^{Scd1} (760-872) showed a specific binding towards the GTP-loaded Ras1.G17V (1-172)
425 (Fig. 7C). However, the binding of Ras1.G17V^{GTP} to MAPKKK^{Byr2} was substantially decreased
426 when the Cdc42-GEF^{Scd1} fragment was added (Fig. 7D). The result likely refects the intrinsic
427 biochemical competitive nature of MAPKKK^{Byr2} and Cdc42-GEF^{Scd1} for Ras1 binding. As we show
428 below, this simple hypothesis successfully describes pheromone signalling mutants tested in this

429 study, suggesting that no unproven cross links are necessary to reproduce the *in vivo*
430 observations.
431 An intriguing common feature observed in both Cdc42-GEF^{scd1}Δ and *ras1.G17V* mutants is that
432 **pp**MAPK^{Spk1} peaks not only at an earlier time point, but also with a *lower amplitude* as
433 compared to the wildtype. If increased Ras1^{GTP} levels simply accelerate MAPK^{Spk1} activation, as
434 has been conventionally assumed, **pp**MAPK^{Spk1} production should peak earlier *and higher*
435 (Supplementary Fig S6B, best fit out of 1000 global fits), and the addition of Ras1^{GTP} only should
436 increase the amplitude, but not affect timing (Supplementary Fig S6C). We confirmed these
437 results in the best models from 1000 global fits (Materials and Methods). The comparison
438 between our experimental results and the *in silico* predictions suggests that the role of Ras1^{GTP}
439 is more complex than previously thought.
440 Strikingly, if we hypothesize that Ras1^{GTP} also contributes to the negative feedback [L10] (Fig.
441 7A), we recapitulate the "*earlier and lower*" peak of **pp**MAPK^{Spk1} in both the *ras1.G17V* and the
442 Cdc42-GEF^{scd1}Δ mutants (Fig. 7B). We currently do not have a direct experimental evidence to
443 support [L10]. However, considering the fact that Ras1^{GTP} likely acts as a physical signalling hub
444 at the cell cortex, mediating MAPKKK^{Byr2} recruitment and activation, which leads to recruitment
445 of MAPKK^{Byr1} and MAPK^{Spk1}, Ras1^{GTP} may work as a two-way amplifier, both assisting localized
446 MAPK^{Spk1} activation at the shmoo site, as well as helping the negative feedback by concentrating
447 the affected molecules.
448 The model successfully recapitulated the experimental results for wildtype, *ras1.G17V*,
449 MAPKK$^{Byr1.DD}$ and *cdc42-GEF^{scd1}Δ* mutants (Fig. 7B). To test the predictive capacity of the model,
450 we next performed an *in silico* experiment where we titrated increasing amounts of Ras1^{GTP} in
451 the wildtype condition before nitorgen removal. In agreement with our hypothesis, we obtained
452 a *ras1.G17V*-like **pp**MAPK^{Spk1} activation profile with increasing amount of Ras1^{GTP}, i.e., the
453 **pp**MAPK^{Spk1} peaks earlier with a lower peak intensity (Fig. 7E). The result further supported that
454 Ras1^{GTP} availability alone is sufficient to explain both the *ras1.G17V* and *Cdc42-GEF^{scd1}Δ*
455 phenotypes.
456 To further test the predictive value of the model, we asked whether it could predict **pp**MAPK^{Spk1}
457 dynamics in the 21 other strains, which were measured (Fig. 2-6), but not used for fitting the
458 model. We implemented each mutation in the wildtype model (Supplementary Table S2) and
459 the model accurately predicted relative **pp**MAPK^{Spk1} dynamics in 17 cases, or showed
460 predicitons in close proximity to the observed **pp**MAPK^{Spk1} dynamics in the 4 remaining cases

461 (Fig. 7F). Concluding from these results, our model likely represents the physiological framework
462 of fission yeast RAS-MAPK signalling.
463
464 **Discussion**
465
466 By quantitating the MAPK^{Spk1} and Cdc42 activation status during the mating process and
467 conducting epistasis analysis between numerous signalling mutants, we showed that Ras1
468 coordinates activation of both the MAPK^{Spk1} cascade and the Cdc42 pathway. Furthermore, we
469 revealed that the *ras1.G17V* mutant phenotype is caused by deregulation of Cdc42, rather than
470 altered activation of MAPK^{Spk1} in physiological setting. Based on the experimental data, we built
471 a mathematical model, which hypothesize that the MAPK^{Spk1} cascade is subject to robust
472 feedback regulation and two Ras1 effectors, Cdc42-GEF^{Scd1} and MAPKKK^{Byr2}, are competing for
473 active Ras1. This model faithfully recapitulates MAPK^{Spk1} activation profiles in the wildtype and
474 all mutant strains examined in this study. The model implies that targeting one of the RAS
475 effector pathways can potentially result in a complex outcome, rather than simply shutting
476 down the targeted effector pathway. We concluded that fission yeast pheromone Ras signalling
477 is not only defined by compartmentalisation (Onken et al., 2006) but rather a coordination of
478 events involving both the MAPK^{Spk1} and Cdc42 pathways.
479 In this study, we confirmed that Gpa1 is the central player of the pheromone signalling. It is
480 likely that Gpa1 is the most downstream molecule conveying the complete pheromone signal.
481 Considering that all the pheromone signalling components examined so far have been found at
482 the shmoo site (Dudin et al., 2016; Merlini et al., 2016; Merlini et al., 2018)(this study), an
483 attractive hypothesis is as follows: firstly, the activated pheromone receptor Map3/Mam2
484 locally activates Gpa1, which activates Ras1 and MAPK^{Spk1}. This then leads to a localised
485 activation of the Cdc42, causing shmoo formation in the direction of a mating partner (Fig. 7G).
486 The *ras1.G17V* mutation led to a acute activation of MAPK^{Spk1} compared with the wildtype cells.
487 The G17V mutantion of Ras1 is equivalent of G12V mutation of mammalian RAS, which results
488 in a substantial reduction of both intrinsic and GAP-mediated GTPase activities (Trahey and
489 McCormick, 1987). Therefore a larger fraction of Ras1 is expected to be in the GTP-bound form
490 in the *ras1.G17V* mutant cells. By mathematical modelling, we showed that the increased
491 Ras1^{GTP} pool can explain a faster acute activation of MAPK^{Spk1}.

492 To our surprise, the constitutive Ras1.G17V mutation did not induce over-activation of
493 MAPK^{Spk1}. The attenuated MAPK^{Spk1} activation in the presence of Ras1.G17V indicated that an
494 efficient feedback mechanism is in place to counteract the effect of Ras1.G17V. Strikingly, the
495 same trend has been reported in the mouse model of the *K-ras^{G12D}* mutation integrated at the
496 endogenous chromosome locus (Tuveson et al., 2004). Therefore it is highly likely that the
497 MAPK cascade is generally robust against upstream oncogenic constitutive stimulation.
498 Based on our observation that the MAPK^{Spk1} is constitutively activated in the *MAPKK$^{byr1.DD}$*
499 mutant, we predict that the negative regulation occurs upstream of, or at the same level as,
500 MAPKK^{Byr1}, rather than phosphatases that directly regulate MAPK^{Spk1}. In humans, ERK is shown
501 to phosphorylate RAF proteins, the prototype MAPKKKs, to contribute to ERK signal attenuation
502 (Brummer et al., 2003; Dougherty et al., 2005; Ritt et al., 2010). In future studies it will be
503 important to determine whether MAPK^{Spk1} can directly downregulate MAPKKK^{Byr2} in a
504 physiological setting.
505 Our results also show that an adaptor^{Ste4} plays a crucial role in activating MAPKKK^{Byr2}, abolishing
506 **pp**MAPK^{Spk1} production even in the presence of *ras1.G17V* mutation. This suggests that the
507 adaptor^{Ste4} fits well to be one of the major targets by the negative feedback loop against
508 **pp**MAPK^{Spk1}. This mechanism is shared by budding yeast, where an adaptor protein, Ste50,
509 modulates MAPKKK^{Ste11} (Ramezani-Rad, 2003). In humans, although such an adaptor protein for
510 RAF proteins has yet to be identified, multiple RAF-interacting proteins, including 14-3-3
511 proteins, as well as formation of heterodimers between BRAF and CRAF, have been studied for
512 their Ras-independent mechanism to activate RAF proteins (Lavoie and Therrien, 2015).
513 Collectively, MAPK cascades seem to retain a general resistance to oncogenic RAS mutations in
514 physiological settings.
515 Whilst lack of Cdc42 activation does not impair MAPK^{Spk1} activation, we found that MAPK^{Spk1}
516 activity is required for shmoo formation even in the presence of Ras1.G17V (Fig. 2C). Therefore,
517 the two Ras1 effectors, Cdc42 and MAPK^{Spk1} pathways, are not completely separable. The
518 situation is reminiscent of the *K-ras^{G12D}* MEFs (Tuveson et al., 2004). In this system, the *K-ras^{G12D}*
519 MEFs showed morphological anomalies. As both ERK and AKT phosphorylation levels in the *K-*
520 *ras^{G12D}* MEFs resembled wildtype, these pathways unlikely caused the morphological
521 phenotype. Nonetheless, inhibitors against MAPK and PI3K pathways reverted the *K-ras^{G12D}*–
522 induced abnormal morphology back to the one similar to wildtype. The observation suggests
523 that MAPK and PI3K pathways somehow contribute to the *K-ras^{G12D}* morphological phenotype;

524 for example, a basal level of MAPK and PI3K pathway activation may be a prerequisite for the *K-*
525 *ras*^{G12D}–induced morphological anomalies.
526 The molecular mechanism of how MAPK^{Spk1} contributes to Cdc42 activation will require further
527 studies. Key components in pheromone signalling are transcriptionally up-regulated upon
528 pheromone signalling (Xue-Franzen et al., 2006). This is driven by MAPK^{Spk1}, which activates the
529 master transcriptional regulator Ste11 (Kjaerulff et al., 2005; Mata and Bahler, 2006; Xue-
530 Franzen et al., 2006). Therefore, the contribution of MAPK^{Spk1} to Cdc42 activation is expected to
531 occur, at least partly, through transcriptional activation.
532 In addition, localisation of signalling components may be regulated by MAPK^{Spk1}. In budding
533 yeast, Cdc24, the GEF for Cdc42, is sequestered into the nucleus by an adaptor protein Far1
534 (Nern and Arkowitz, 2000; Shimada et al., 2000). Upon the pheromone signalling, budding yeast
535 MAPK^{Fus3} phosphorylates Far1, which then brings Cdc24 out to the shmoo site, leading to Cdc42
536 activation on the cell cortex (Hegemann et al., 2015).
537 MAPK^{Spk1} may also directly phosphorylate to activate Cdc42 and/or its regulatory proteins such
538 as Cdc42-GEF^{Scd1}, Scd2 or GAP-Cdc42^{Rga4}, all of which function at the shmoo site during the
539 mating (Bendezu and Martin, 2013; Dudin et al., 2016)(Fig.4 A and B). In agreement with this
540 hypothesis, a transient MAPK^{Spk1} and MAPKK^{Byr1} signal on the cell cortex was observed during
541 the mating process (Fig. 1)(Dudin et al., 2016). Localisation of MAPK at the growing cell tips was
542 also observed in other fungi including *S. cerevisiae* and *N. crassa* (Chen et al., 2010; Fleissner et
543 al., 2009; Maeder et al., 2007; van Drogen et al., 2001). In budding yeast, MAPK^{Fus3} can directly
544 phosphorylates Bni1, a formin that organises actin filaments, to facilitate shmoo formation
545 (Matheos et al., 2004).
546 Interestingly, during the vegetative growth when expression of MAPK^{Spk1} is repressed,
547 Ras1.G17V is still capable of activating Cdc42 (Fig. 4C and D). Whether other MAPKs, such as
548 Sty1 or Pmk1, contribute to Cdc42 activation during the vegetative cell cycle will be an
549 important question to answer. Intriguingly, recent studies show that Sty1 inhibits, rather than
550 assists, establishment of the Cdc42 polarity module (Mutavchiev et al., 2016). Collectively, it is
551 likely that the Cdc42 polarity module is regulated in a context dependent manner by multiple
552 MAPKs in a range of ways.
553 In this study we revealed the vital contribution of Cdc42 to induce the *ras1.G17V* phenotype in
554 fission yeast pheromone signalling. In mouse models, small GTPases, Cdc42 and Rac, are
555 required for *H-ras*^{G12V} induced transformation (Malliri et al., 2002; Stengel and Zheng, 2012).

Therefore, oncogenic RAS-induced Cdc42/Rac misregulation may be a common basis of oncogenicity of mutated-RAS-induced signalling. Specifically targeting this process may therefore be an effective strategy against oncogenic RAS-driven tumourigenesis.

Acknowledgment

The authors thank Tatsuya Maeda, Thibault Mayor, Janni Petersen, Louise Fairall, John Schwabe, David Critchley, Andrey Reviyakin, Gary Willars and Mohan Harihar for helpful suggestions, stimulating discussions and critical reading of the manuscript. We thank PROTEX and PNACL at University of Leicester for their technical assistance. We are grateful to Kazu Shiozaki, Keith Gull and Yeast Genetic Resource Center for providing strains and antibodies. This work was funded by the Wellcome Trust Institutional Strategic Support Fund WT097828/Z/11/Z, WT097828/Z/11/B and the Deutsche Forschungsgemeinschaft (DFG) EXC 81. A.V. was supported by German Academic Exchange Service (DAAD) A0981674.

Author Contributions

E.J.K., S.R. and K.T. generated yeast strains. E.J.K., G.S. and K.T. monitored activation status of $MAPK^{Spk1}$ and Cdc42. A.V. and E.K. conducted mathematical modelling. E.J.K., K.S. and K.T. conducted image analysis. M.T., R.G., C.P. and C.D. conducted biochemical analysis of Ras1, Byr2 and Scd1. E.J.K., A.V., E.K. and K.T. designed the experiments and interpreted the data.

Declaration of Interests

The authors declare no competing interests.

References

Barr, M.M., Tu, H., Van Aelst, L., and Wigler, M. (1996). Identification of Ste4 as a potential regulator of Byr2 in the sexual response pathway of Schizosaccharomyces pombe. Mol Cell Biol *16*, 5597-5603.

Bendezu, F.O., and Martin, S.G. (2013). Cdc42 explores the cell periphery for mate selection in fission yeast. Current biology : CB *23*, 42-47.

Bitton, D.A., Grallert, A., Scutt, P.J., Yates, T., Li, Y., Bradford, J.R., Hey, Y., Pepper, S.D., Hagan, I.M., and Miller, C.J. (2011). Programmed fluctuations in sense/antisense transcript ratios drive sexual differentiation in S. pombe. Mol Syst Biol *7*, 559.

589 Brummer, T., Naegele, H., Reth, M., and Misawa, Y. (2003). Identification of novel ERK-
590 mediated feedback phosphorylation sites at the C-terminus of B-Raf. Oncogene *22*, 8823-
591 8834.
592 Chang, E.C., Barr, M., Wang, Y., Jung, V., Xu, H.P., and Wigler, M.H. (1994). Cooperative
593 interaction of S. pombe proteins required for mating and morphogenesis. Cell *79*, 131-141.
594 Chen, R.E., Patterson, J.C., Goupil, L.S., and Thorner, J. (2010). Dynamic localization of Fus3
595 mitogen-activated protein kinase is necessary to evoke appropriate responses and avoid
596 cytotoxic effects. Mol Cell Biol *30*, 4293-4307.
597 Cox, A.D., and Der, C.J. (2010). Ras history: The saga continues. Small GTPases *1*, 2-27.
598 Das, M., Wiley, D.J., Medina, S., Vincent, H.A., Larrea, M., Oriolo, A., and Verde, F. (2007).
599 Regulation of cell diameter, For3p localization, and cell symmetry by fission yeast Rho-GAP
600 Rga4p. Molecular biology of the cell *18*, 2090-2101.
601 Didmon, M., Davis, K., Watson, P., Ladds, G., Broad, P., and Davey, J. (2002). Identifying
602 regulators of pheromone signalling in the fission yeast Schizosaccharomyces pombe.
603 Current genetics *41*, 241-253.
604 Dougherty, M.K., Muller, J., Ritt, D.A., Zhou, M., Zhou, X.Z., Copeland, T.D., Conrads, T.P.,
605 Veenstra, T.D., Lu, K.P., and Morrison, D.K. (2005). Regulation of Raf-1 by direct feedback
606 phosphorylation. Mol Cell *17*, 215-224.
607 Dudin, O., Merlini, L., and Martin, S.G. (2016). Spatial focalization of pheromone/MAPK
608 signaling triggers commitment to cell-cell fusion. Genes Dev *30*, 2226-2239.
609 Endo, M., Shirouzu, M., and Yokoyama, S. (2003). The Cdc42 binding and scaffolding
610 activities of the fission yeast adaptor protein Scd2. J Biol Chem *278*, 843-852.
611 Fleissner, A., Leeder, A.C., Roca, M.G., Read, N.D., and Glass, N.L. (2009). Oscillatory
612 recruitment of signaling proteins to cell tips promotes coordinated behavior during cell
613 fusion. Proceedings of the National Academy of Sciences of the United States of America
614 *106*, 19387-19392.
615 Fukui, Y., Kozasa, T., Kaziro, Y., Takeda, T., and Yamamoto, M. (1986). Role of a ras homolog
616 in the life cycle of Schizosaccharomyces pombe. Cell *44*, 329-336.
617 Fukui, Y., Miyake, S., Satoh, M., and Yamamoto, M. (1989). Characterization of the
618 Schizosaccharomyces pombe ral2 gene implicated in activation of the ras1 gene product.
619 Mol Cell Biol *9*, 5617-5622.
620 Gronwald, W., Huber, F., Grunewald, P., Sporner, M., Wohlgemuth, S., Herrmann, C., and
621 Kalbitzer, H.R. (2001). Solution structure of the Ras binding domain of the protein kinase
622 Byr2 from Schizosaccharomyces pombe. Structure *9*, 1029-1041.
623 Hegemann, B., Unger, M., Lee, S.S., Stoffel-Studer, I., van den Heuvel, J., Pelet, S., Koeppl, H.,
624 and Peter, M. (2015). A Cellular System for Spatial Signal Decoding in Chemical Gradients.
625 Dev Cell *35*, 458-470.
626 Hirota, K., Tanaka, K., Watanabe, Y., and Yamamoto, M. (2001). Functional analysis of the C-
627 terminal cytoplasmic region of the M-factor receptor in fission yeast. Genes Cells *6*, 201-
628 214.
629 Hoops, S., Sahle, S., Gauges, R., Lee, C., Pahle, J., Simus, N., Singhal, M., Xu, L., Mendes, P., and
630 Kummer, U. (2006). COPASI--a COmplex PAthway SImulator. Bioinformatics *22*, 3067-3074.
631 Hughes, D.A., Fukui, Y., and Yamamoto, M. (1990). Homologous activators of ras in fission
632 and budding yeast. Nature *344*, 355-357.
633 Hughes, D.A., Yabana, N., and Yamamoto, M. (1994). Transcriptional regulation of a Ras
634 nucleotide-exchange factor gene by extracellular signals in fission yeast. J Cell Sci *107 (Pt*
635 *12)*, 3635-3642.
636 Imai, Y., and Yamamoto, M. (1992). Schizosaccharomyces pombe sxa1+ and sxa2+ encode
637 putative proteases involved in the mating response. Mol Cell Biol *12*, 1827-1834.

638 Kelly, F.D., and Nurse, P. (2011). Spatial control of Cdc42 activation determines cell width in
639 fission yeast. Molecular biology of the cell *22*, 3801-3811.
640 Kjaerulff, S., Andersen, N.R., Borup, M.T., and Nielsen, O. (2007). Cdk phosphorylation of the
641 Ste11 transcription factor constrains differentiation-specific transcription to G1. Genes Dev
642 *21*, 347-359.
643 Kjaerulff, S., Lautrup-Larsen, I., Truelsen, S., Pedersen, M., and Nielsen, O. (2005).
644 Constitutive activation of the fission yeast pheromone-responsive pathway induces ectopic
645 meiosis and reveals ste11 as a mitogen-activated protein kinase target. Mol Cell Biol *25*,
646 2045-2059.
647 Lavoie, H., and Therrien, M. (2015). Regulation of RAF protein kinases in ERK signalling. Nat
648 Rev Mol Cell Biol *16*, 281-298.
649 Lin, A.W., Barradas, M., Stone, J.C., van Aelst, L., Serrano, M., and Lowe, S.W. (1998).
650 Premature senescence involving p53 and p16 is activated in response to constitutive
651 MEK/MAPK mitogenic signaling. Genes Dev *12*, 3008-3019.
652 Maeder, C.I., Hink, M.A., Kinkhabwala, A., Mayr, R., Bastiaens, P.I., and Knop, M. (2007).
653 Spatial regulation of Fus3 MAP kinase activity through a reaction-diffusion mechanism in
654 yeast pheromone signalling. Nat Cell Biol *9*, 1319-1326.
655 Malliri, A., van der Kammen, R.A., Clark, K., van der Valk, M., Michiels, F., and Collard, J.G.
656 (2002). Mice deficient in the Rac activator Tiam1 are resistant to Ras-induced skin tumours.
657 Nature *417*, 867-871.
658 Marcus, S., Polverino, A., Chang, E., Robbins, D., Cobb, M.H., and Wigler, M.H. (1995). Shk1, a
659 homolog of the Saccharomyces cerevisiae Ste20 and mammalian p65PAK protein kinases, is
660 a component of a Ras/Cdc42 signaling module in the fission yeast Schizosaccharomyces
661 pombe. Proceedings of the National Academy of Sciences of the United States of America *92*,
662 6180-6184.
663 Masuda, T., Kariya, K., Shinkai, M., Okada, T., and Kataoka, T. (1995). Protein kinase Byr2 is a
664 target of Ras1 in the fission yeast Schizosaccharomyces pombe. J Biol Chem *270*, 1979-
665 1982.
666 Mata, J., and Bahler, J. (2006). Global roles of Ste11p, cell type, and pheromone in the control
667 of gene expression during early sexual differentiation in fission yeast. Proceedings of the
668 National Academy of Sciences of the United States of America *103*, 15517-15522.
669 Mata, J., Lyne, R., Burns, G., and Bahler, J. (2002). The transcriptional program of meiosis
670 and sporulation in fission yeast. Nature genetics *32*, 143-147.
671 Mata, J., Wilbrey, A., and Bahler, J. (2007). Transcriptional regulatory network for sexual
672 differentiation in fission yeast. Genome biology *8*, R217.
673 Matheos, D., Metodiev, M., Muller, E., Stone, D., and Rose, M.D. (2004). Pheromone-induced
674 polarization is dependent on the Fus3p MAPK acting through the formin Bni1p. J Cell Biol
675 *165*, 99-109.
676 Merlini, L., Dudin, O., and Martin, S.G. (2013). Mate and fuse: how yeast cells do it. Open Biol
677 *3*, 130008.
678 Merlini, L., Khalili, B., Bendezu, F.O., Hurwitz, D., Vincenzetti, V., Vavylonis, D., and Martin,
679 S.G. (2016). Local Pheromone Release from Dynamic Polarity Sites Underlies Cell-Cell
680 Pairing during Yeast Mating. Current biology : CB *26*, 1117-1125.
681 Merlini, L., Khalili, B., Dudin, O., Michon, L., Vincenzetti, V., and Martin, S.G. (2018).
682 Inhibition of Ras activity coordinates cell fusion with cell-cell contact during yeast mating. J
683 Cell Biol *217*, 1467-1483.
684 Mutavchiev, D.R., Leda, M., and Sawin, K.E. (2016). Remodeling of the Fission Yeast Cdc42
685 Cell-Polarity Module via the Sty1 p38 Stress-Activated Protein Kinase Pathway. Current
686 biology : CB *26*, 2921-2928.

687 Nadin-Davis, S.A., and Nasim, A. (1988). A gene which encodes a predicted protein kinase
688 can restore some functions of the ras gene in fission yeast. EMBO J *7*, 985-993.
689 Nadin-Davis, S.A., Nasim, A., and Beach, D. (1986a). Involvement of ras in sexual
690 differentiation but not in growth control in fission yeast. EMBO J *5*, 2963-2971.
691 Nadin-Davis, S.A., Yang, R.C., Narang, S.A., and Nasim, A. (1986b). The cloning and
692 characterization of a RAS gene from Schizosaccharomyces pombe. J Mol Evol *23*, 41-51.
693 Nern, A., and Arkowitz, R.A. (2000). Nucleocytoplasmic shuttling of the Cdc42p exchange
694 factor Cdc24p. J Cell Biol *148*, 1115-1122.
695 Obara, T., Nakafuku, M., Yamamoto, M., and Kaziro, Y. (1991). Isolation and characterization
696 of a gene encoding a G-protein alpha subunit from Schizosaccharomyces pombe:
697 involvement in mating and sporulation pathways. Proceedings of the National Academy of
698 Sciences of the United States of America *88*, 5877-5881.
699 Okazaki, N., Okazaki, K., Tanaka, K., and Okayama, H. (1991). The ste4+ gene, essential for
700 sexual differentiation of Schizosaccharomyces pombe, encodes a protein with a leucine
701 zipper motif. Nucleic acids research *19*, 7043-7047.
702 Onken, B., Wiener, H., Philips, M.R., and Chang, E.C. (2006). Compartmentalized signaling of
703 Ras in fission yeast. Proceedings of the National Academy of Sciences of the United States of
704 America *103*, 9045-9050.
705 Ottilie, S., Miller, P.J., Johnson, D.I., Creasy, C.L., Sells, M.A., Bagrodia, S., Forsburg, S.L., and
706 Chernoff, J. (1995). Fission yeast pak1+ encodes a protein kinase that interacts with Cdc42p
707 and is involved in the control of cell polarity and mating. EMBO J *14*, 5908-5919.
708 Ozoe, F., Kurokawa, R., Kobayashi, Y., Jeong, H.T., Tanaka, K., Sen, K., Nakagawa, T., Matsuda,
709 H., and Kawamukai, M. (2002). The 14-3-3 proteins Rad24 and Rad25 negatively regulate
710 Byr2 by affecting its localization in Schizosaccharomyces pombe. Mol Cell Biol *22*, 7105-
711 7119.
712 Papadaki, P., Pizon, V., Onken, B., and Chang, E.C. (2002). Two ras pathways in fission yeast
713 are differentially regulated by two ras guanine nucleotide exchange factors. Mol Cell Biol *22*,
714 4598-4606.
715 Pereira, P.S., and Jones, N.C. (2001). The RGS domain-containing fission yeast protein,
716 Rgs1p, regulates pheromone signalling and is required for mating. Genes Cells *6*, 789-802.
717 Prior, I.A., Lewis, P.D., and Mattos, C. (2012). A comprehensive survey of Ras mutations in
718 cancer. Cancer Res *72*, 2457-2467.
719 Qiu, R.G., Abo, A., McCormick, F., and Symons, M. (1997). Cdc42 regulates anchorage-
720 independent growth and is necessary for Ras transformation. Mol Cell Biol *17*, 3449-3458.
721 Ramachander, R., Kim, C.A., Phillips, M.L., Mackereth, C.D., Thanos, C.D., McIntosh, L.P., and
722 Bowie, J.U. (2002). Oligomerization-dependent association of the SAM domains from
723 Schizosaccharomyces pombe Byr2 and Ste4. J Biol Chem *277*, 39585-39593.
724 Ramezani-Rad, M. (2003). The role of adaptor protein Ste50-dependent regulation of the
725 MAPKKK Ste11 in multiple signalling pathways of yeast. Current genetics *43*, 161-170.
726 Ritt, D.A., Monson, D.M., Specht, S.I., and Morrison, D.K. (2010). Impact of feedback
727 phosphorylation and Raf heterodimerization on normal and mutant B-Raf signaling. Mol
728 Cell Biol *30*, 806-819.
729 Schubbert, S., Bollag, G., and Shannon, K. (2007). Deregulated Ras signaling in
730 developmental disorders: new tricks for an old dog. Curr Opin Genet Dev *17*, 15-22.
731 Shimada, Y., Gulli, M.-P., and Peter, M. (2000). Nuclear sequestration of the exchange factor
732 Cdc24 by Far1 regulates cell polarity during yeast mating. Nature Cell Biology *2*, 117.
733 Sipiczki, M. (1988). The role of sterility genes (ste and aff) in the initiation of sexual
734 development in Schizosaccharomyces pombe. Molecular & general genetics : MGG *213*, 529-
735 534.

736 Stengel, K.R., and Zheng, Y. (2012). Essential role of Cdc42 in Ras-induced transformation
737 revealed by gene targeting. PLoS One *7*, e37317.
738 Sugimoto, A., Iino, Y., Maeda, T., Watanabe, Y., and Yamamoto, M. (1991).
739 Schizosaccharomyces pombe ste11+ encodes a transcription factor with an HMG motif that
740 is a critical regulator of sexual development. Genes Dev *5*, 1990-1999.
741 Tatebe, H., Nakano, K., Maximo, R., and Shiozaki, K. (2008). Pom1 DYRK regulates
742 localization of the Rga4 GAP to ensure bipolar activation of Cdc42 in fission yeast. Current
743 biology : CB *18*, 322-330.
744 Toda, T., Shimanuki, M., and Yanagida, M. (1991). Fission yeast genes that confer resistance
745 to staurosporine encode an AP-1-like transcription factor and a protein kinase related to
746 the mammalian ERK1/MAP2 and budding yeast FUS3 and KSS1 kinases. Genes Dev *5*, 60-
747 73.
748 Trahey, M., and McCormick, F. (1987). A cytoplasmic protein stimulates normal N-ras p21
749 GTPase, but does not affect oncogenic mutants. Science *238*, 542-545.
750 Tratner, I., FourticqEsqueoute, A., Tillit, J., and Baldacci, G. (1997). Cloning and
751 characterization of the S-pombe gene efc25(+), a new putative guanine nucleotide exchange
752 factor. Gene *193*, 203-210.
753 Tu, H., Barr, M., Dong, D.L., and Wigler, M. (1997). Multiple regulatory domains on the Byr2
754 protein kinase. Mol Cell Biol *17*, 5876-5887.
755 Tuveson, D.A., Shaw, A.T., Willis, N.A., Silver, D.P., Jackson, E.L., Chang, S., Mercer, K.L.,
756 Grochow, R., Hock, H., Crowley, D.*, et al.* (2004). Endogenous oncogenic K-ras(G12D)
757 stimulates proliferation and widespread neoplastic and developmental defects. Cancer Cell
758 *5*, 375-387.
759 van Drogen, F., Stucke, V.M., Jorritsma, G., and Peter, M. (2001). MAP kinase dynamics in
760 response to pheromones in budding yeast. Nat Cell Biol *3*, 1051-1059.
761 Verde, F., Mata, J., and Nurse, P. (1995). Fission yeast cell morphogenesis: identification of
762 new genes and analysis of their role during the cell cycle. J Cell Biol *131*, 1529-1538.
763 Wang, Y., Xu, H.P., Riggs, M., Rodgers, L., and Wigler, M. (1991). byr2, a Schizosaccharomyces
764 pombe gene encoding a protein kinase capable of partial suppression of the ras1 mutant
765 phenotype. Mol Cell Biol *11*, 3554-3563.
766 Watson, P., Davis, K., Didmon, M., Broad, P., and Davey, J. (1999). An RGS protein regulates
767 the pheromone response in the fission yeast Schizosaccharomyces pombe. Mol Microbiol
768 *33*, 623-634.
769 Weston, C., Bond, M., Croft, W., and Ladds, G. (2013). The coordination of cell growth during
770 fission yeast mating requires Ras1-GTP hydrolysis. PLoS One *8*, e77487.
771 Xu, H.P., White, M., Marcus, S., and Wigler, M. (1994). Concerted action of RAS and G
772 proteins in the sexual response pathways of Schizosaccharomyces pombe. Mol Cell Biol *14*,
773 50-58.
774 Xue-Franzen, Y., Kjaerulff, S., Holmberg, C., Wright, A., and Nielsen, O. (2006). Genomewide
775 identification of pheromone-targeted transcription in fission yeast. BMC Genomics *7*, 303.
776 Yamamoto, M. (1996). The molecular control mechanisms of meiosis in fission yeast.
777 Trends Biochem Sci *21*, 18-22.
778 Zheng, C.F., and Guan, K.L. (1994). Activation of MEK family kinases requires
779 phosphorylation of two conserved Ser/Thr residues. EMBO J *13*, 1123-1131.
780 Zhu, J., Woods, D., McMahon, M., and Bishop, J.M. (1998). Senescence of human fibroblasts
781 induced by oncogenic Raf. Genes Dev *12*, 2997-3007.
782

783

784 ## Figure legends

785 **Figure 1. Distinct modes of MAPK^{Spk1} temporal phosphorylation profile and morphological**
786 **changes during sexual differentiation in wildtype, *MAPKK$^{byr1.DD}$* and *ras1.G17V* mutants.**

787 (A) A pictorial representation of wildtype fission yeast sexual differentiation. (B) A list of key
788 signalling components of the fission yeast pheromone signalling pathway. The diagram reflects
789 the prediction that Gpa1 and Ras1 separately contribute to activation of MAPKKK^{Byr2} activation
790 although the precise mechanism is unknown (Xu et al., 1994). At the same time, Ras1 activation
791 is expected to be at least partly under influence of active Gpa1 because the *ste6* gene, encoding
792 a Ras1 activator, is strongly induced upon successful pheromone signaling (Hughes et al., 1994).
793 (C)-(H) Cells were induced for sexual differentiation by the plate mating assay system as
794 described in the materials and methods. (C), (E) and (G) Quantified **pp**MAPK^{Spk1} signal from
795 western blots of wildtype (KT3082) (C), *MAPKK$^{byr1.DD}$* (KT3435) (E) and *ras1.G17V* (KT3084) (G)
796 cells. Three biological replicates were used for quantitation (error bars are ±SEM). α-tubulin was
797 used as a loading control and quantitation was carried out using the Image Studio ver2.1
798 software (Licor Odyssey CLx Scanner). For the wildtype samples in (C), the % of cells mating is
799 also indicated. The wildtype **pp**MAPK^{Spk1} result (C) is also presented in (E) and (G) as a reference.
800 (D), (F) and (H) Cellular morphology (brightfield) and localization of MAPK^{Spk1}-GFP over a 24 hour
801 time-course in wildtype (D), *MAPKK$^{byr1.DD}$* (F) and *ras1.G17V* (H) cells. Time after induction of
802 mating in hours is indicated on the left. At each time point, a bright-field image and a GFP signal
803 image were taken and processed as described in materials and methods. Green asterisks in the
804 time 24 h in the *ras1.G17V* cell image (H) indicate auto-fluorescence signal from inviable cell
805 debris, which were presumably produced through cytokinesis failure or cell lysis. Yellow arrows
806 in panels (D) and (F) indicate transient accumulation of MAPK^{Spk1}-GFP at the shmoo tips. Scale
807 bars represent 10µm.

808

809 **Figure 2. In the *ras1.G17V MAPKK$^{byr1.DD}$* double mutant, the MAPK^{Spk1} phosphorylation profile**
810 **follows *MAPKK$^{byr1.DD}$* single mutant phenotype whilst cell morphology mimics the *ras1.G17V***
811 **single mutant phenotype.**

812 (A) MAPK^{Spk1} phosphorylation status in the *ras1.G17V MAPKK$^{byr1.DD}$* double mutant cells
813 (KT3439). Cells were induced for mating by the plate mating assay system as described in the
814 materials and methods. Quantitated **pp**MAPK^{Spk1} signal (arbitrary unit) from western blots is

815 presented. Results of two biological replicates (each derived from three technical replicates,
816 error bars are ±SEM) are presented in red. (B) The terminal mating phenotype of *ras1.G17V*
817 *MAPKK*$^{byr1.DD}$ double mutant is a phenocopy of *ras1.G17V* single mutant which shows the
818 "elongated" morphology. Images were taken of *ras1.G17V MAPKK*$^{byr1.DD}$ double mutant
819 (KT3439) in the same way as in Fig. 1. Time after induction of mating in hours is indicated on the
820 left. (C) There is no morphological change in the absence of MAPK^{Spk1} signalling. Cell images of
821 *MAPKK*^{byr1}*Δ* (KT4700) and *ras1.G17V MAPKK*^{byr1}*Δ* (KT5030) strains are shown. Images were
822 taken in the same way as in Fig. 1. Time after induction of mating in hours is indicated on the
823 left of each series. Scale bars represent 10µm.

824

825 **Figure 3. Ras1 activates both MAPK^{Spk1} and Cdc42 pathways during pheromone signalling.**

826 (A) *scd1Δ* morphology and MAPK^{Spk1}-GFP signal. Images of WT (KT3082), *scd1Δ* (KT4061) and
827 *scd1Δ ras1.G17V* double mutant (KT4056) were taken in the same way as in Fig.1. Numbers on
828 the left represents hours after induction of mating. (B) MAPK^{Spk1} phosphorylation state in *scd1Δ*
829 (KT4061) cells after mating induction. Results of three biological replicates (error bars are ±SEM)
830 are presented. The wildtype **pp**MAPK^{Spk1} result presented in Fig.1 (C) is also shown in blue as a
831 reference. (C) Cell images of *scd1Δ MAPKK*$^{byr1.DD}$ double mutant (KT4047) were taken in the
832 same way as in Fig.1. Numbers on the left represents hours after induction of mating. (D)
833 MAPK^{Spk1} phosphorylation state in *ras1Δ* (KT4323), *MAPKK*$^{byr1.DD}$ (KT3435) and *ras1Δ*
834 *MAPKK*$^{byr1.DD}$ (KT4359) cell extracts. Original Western blotting data is presented in Fig. S3A. (E)
835 MAPK^{Spk1} phosphorylation state in *mapkkk*^{byr2}*Δ* (KT3763), *MAPKK*$^{byr1.DD}$ (KT3435) and
836 *mapkkk*^{byr2}*Δ MAPKK*$^{byr1.DD}$ (KT4010) cell extracts. Original Western blotting data is presented in
837 Fig. S3B. For (D) and (E), quantification was carried out using the Image Studio ver2.1 (Li-cor). (F)
838 Cell images of the strains mentioned in (D) and (E) were taken in the same way as in Fig.1.
839 Numbers on the left represents hours after induction of mating. For all the images presented in
840 (A), (C) and (F), scale bars represent 10µm.

841

842 **Figure 4. Ras1.G17V induces cortical Cdc42^{GTP} accumulation**

843 (A) Cell morphology and localisation of Cdc42^{GTP}, indicated by CRIB-GFP signal, during the sexual
844 differentiation process. Wildtype (KT5077) and *ras1.G17V* (KT5082) mutant cells were induced
845 for mating/sexual differentiation by the plate mating assay condition (Materials and Methods)

846 and live cell images were taken at the indicated time after induction of mating/sexual
847 differentiation. Representative CRIB-GFP signal images are presented. Cells with cortical CRIB-
848 GFP foci are indicated by orange stars. Rapidly-disappearing CRIB-GFP signals at the fusion site
849 of wildtype mating cells are indicated by green arrows at time 8.5h image. Scale bar: 10 µm. (B)
850 Quantitation of the results presented in (A). At each time point (4.5h, 6.5h, 10.5h, 12.5h and
851 22.5h after induction of mating/sexual differentiation), 150 cells were examined whether they
852 have cortical CRIB-GFP foci. % cells with cortical CRIB-GFP foci is presented. The experiment was
853 repeated for three times and the mean values and SDs are plotted in the graph. (C) Cell
854 morphology and localisation of $Cdc42^{GTP}$, indicated by CRIB-GFP signal, during vegetative
855 growth. Representative CRIB-GFP signal images of cells of wildtype (KT5077), *ras1Δ* (5107),
856 *ras1.G17V* (KT5082), *rga4Δ* (5551) and *rga4Δ ras1.G17V* (KT5554) are presented. Scale bar: 10
857 µm. (D) Quantitated CRIB-GFP signals on the cell cortex of cells presented in (C). Intensity of GFP
858 signal on the cell cortex was measured along one of the cell tips as indicated as a magenta
859 dotted line in the example image on the right (Scale bar: 10 µm) as stated in the Materials and
860 Methods. 40 cells without septum were measured for each strain and the average curve from all
861 aligned traces per strain was calculated, and displayed with respective standard error of the
862 mean curves (dashed lines) as described in Materials and Methods.

863

864 **Fig. 5. Distinct contributions of Ste4 and Ste6 to $MAPK^{Spk1}$ phosphorylation.**

865 (A) Ste4 is essential for $MAPK^{Spk1}$ activation. $MAPK^{Spk1}$ phosphorylation status in *ste4Δ* (KT4376),
866 *ste4Δ ras1.G17V* (KT5143) and *ste4Δ* $MAPKK^{byr1.DD}$ (KT5136) at times-points 0, 8 ,16 and 24
867 hours post mating induction are presented. Original Western blotting membranes are presented
868 in Fig. S3C. (B) Incapability of *ste4Δ* to cause pheromone-induced morphological change is
869 suppressed by $MAPKK^{byr1.DD}$ but not by *ras1.G17V*. Cell images of *ste4Δ* (KT4376), *ste4Δ*
870 *ras1.G17V* (KT5143) and *ste4Δ* $MAPKK^{byr1.DD}$ (KT5136) strains were taken 24 hours after
871 induction of mating. Scale bar: 10 µm. (C) Lack of Ste6 does not result in the complete loss of
872 $MAPK^{Spk1}$ phosphorylation. $MAPK^{Spk1}$ phosphorylation status in *ste6Δ* (KT4333), *ste6Δ ras1.G17V*
873 (KT4998) and *ste6Δ* $MAPKK^{byr1.DD}$ (KT5139) at times-points 0, 8 ,16 and 24 hours post mating
874 induction are presented. Original Western blotting membranes are presented in Fig. S3D. (D)
875 Incapability of *ste6Δ* to cause pheromone-induced morphological change is suppressed by
876 *ras1.G17V* mutation but not by $MAPKK^{byr1.DD}$ mutation. Cell images of *ste6Δ* (KT4333), *ste6Δ*

877 *ras1.G17V* (KT4998) and *ste6Δ MAPKK*$^{byr1.DD}$ (KT5139) strains were taken 24 hours after
878 induction of mating. Scale bar: 10 µm.

879

880 **Fig. 6. Gpa1 transduces the pheromone signalling by activating MAPK^{Spk1} and Ras1 pathways**

881 (A) MAPK^{Spk1} phosphorylation status in homothallic *gpa1Δ* (KT4335), *gpa1Δ ras1.G17V*
882 (KT5023), *gpa1Δ MAPKK*$^{byr1.DD}$ (KT4353) and *gpa1Δ ras1.val17 MAPKK*$^{byr1.DD}$ (KT5035) at times-
883 points 0, 8 ,12, 16 and 24 hours after mating induction. Original Western membrane is
884 presented in Fig. S4A. (B) Cell images of the above mentioned strains at 16 hours after mating
885 induction. All the cell images were taken and processed as in Figure 1. Scale bar is 10 µm. (C)
886 MAPK^{Spk1} phosphorylation status in *h*$^{-}$ WT (KT4190), *h*$^{-}$ *gpa1.QL* (KT5059), *h*$^{-}$ *ras1.G17V* (KT4233),
887 *h*$^{-}$ *gpa1.QL ras1Δ* (KT5070) and h^{-} *MAPKK*$^{byr1.DD}$ (KT4194) at times-points 0, 8 ,12 and 24 after
888 mating induction. Note that while the activation induced in the *gpa1.QL* mutant was down-
889 regulated, *MAPKK*$^{byr1.DD}$ induced a constitutive activation. Original Western membrane is
890 presented in Fig. S4B. (D) Cell images of the above strains at 12 h after induction of mating. All
891 the cell images were taken and processed as in Figure 1. Scale bar is 10 µm.

892

893 **Fig. 7. Mathematical modelling of the fission yeast pheromone pathway dynamics.**

894 (A) Components and frameworks of the mathematical model in wildtype and signalling mutants:
895 *ras1.G17V*, *Cdc42GEF*^{scd1}*Δ,* and *MAPKK*$^{byr1.DD}$. Changes corresponding to each mutant are
896 indicated as follows: Grey: removed components or interactions, orange: increased level of
897 activity. For the exact implementation of the mutants, see Materials and Method. The
898 measured component, **pp**MAPK^{Spk1}, is highlighted in green. (B) Measured and simulated
899 **pp**MAPK^{Spk1} activation profiles in wildtype, *ras1.G17V*, *Cdc42GEF*^{scd1}*Δ* and *MAPKK*$^{byr1.DD}$ mutants.
900 Dashed lines: model simulations. Diamonds: experimental data presented in Fig. 1C, E, G, and
901 Fig. 3B; error bars: SEM. (C) GTP-loaded Ras1.G17V (1-172) directly binds to Byr2 (65-180) and
902 Scd1 (760-872). *In vitro* GST pull-down assays of bacterially expressed Ras1.G17V (1-172), GST-
903 Byr2 (65-180) and GST-Scd1 (760-872) were conducted as described in materials and methods.
904 GTP-loaded Ras1.G17V (1-172) was found to bind to both GST-Byr2 (65-180) and GST-Scd1 (760-
905 872). (D) Two Ras1 effectors, Byr2 and Scd1, compete for GTP-loaded Ras1.G17V (1-172). In
906 vitro GST pull-down assays of bacterially expressed Ras1.G17V (1-172) and GST-Byr2 (65-180)
907 were conducted as in (A). Addition of Scd1 (760-872) fragment interfered with Ras1-Byr2

908 binding (the 4th lane). Quantitated signal intensities of the Ras1.G17V (1-172) band in the gel are
909 shown in the right panel. (E) Simulated ppMAPK^{Spk1} dynamics in the wildtype model at
910 increasing concentrations of Ras1^{GTP} added *in silico* to the system. Increased Ras1^{GTP}
911 concentration causes advanced and reduced **pp**MAPK^{Spk1} peak intensities. (F) The model fitted
912 to the 4 strains (as above, in red) correctly predicts ppMAPK^{Spk1} dynamics in the additional 21
913 signalling mutant strains measured in this study.(G) Schematic diagram of the fission yeast
914 pheromone signalling pathway, highlighting the branched pheromone sensing, and that
915 ultimately both branches are necessary for mating.

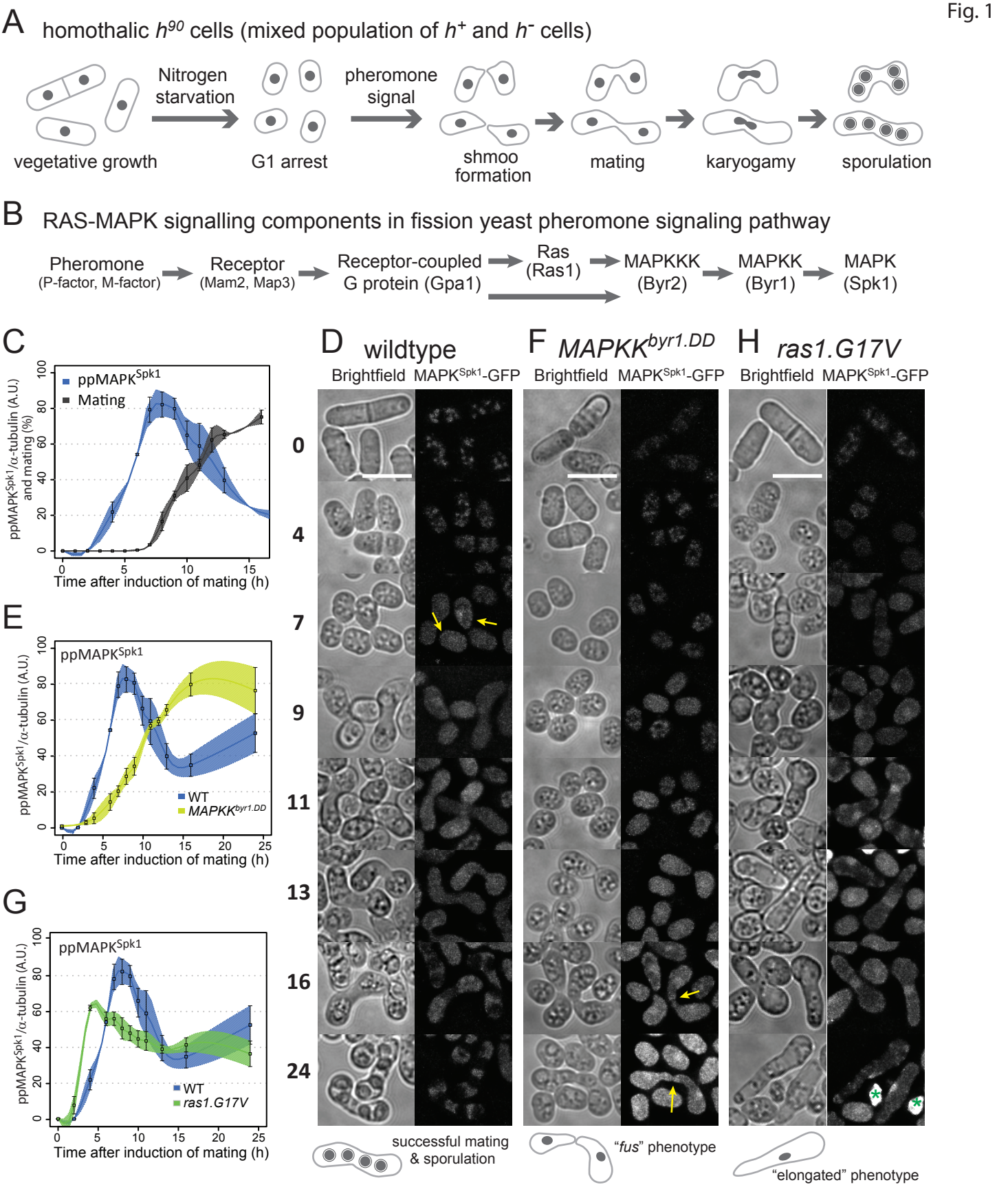

Figure 1. Distinct modes of MAPK^{Spk1} temporal phosphorylation profile and morphological changes during sexual differentiation in wildtype, *MAPKK$^{byr1.DD}$* and *ras1.G17V* mutants.

(A) A pictorial representation of wildtype fission yeast sexual differentiation. (B) A list of key signalling components of the fission yeast pheromone signalling pathway. The diagram reflects the prediction that Gpa1 and Ras1 separately contribute to activation of MAPKKK^{Byr2} activation although the precise mechanism is unknown (Xu et al., 1994). At the same time, Ras1 activation is expected to be at least partly under influence of active Gpa1 because the ste6 gene, encoding a Ras1 activator, is strongly induced upon successful pheromone signaling (Hughes et al., 1994). (C)-(H) Cells were induced for sexual differentiation by the plate mating assay system as described in the materials and methods. (C), (E) and (G) Quantified **pp**MAPK^{Spk1} signal from western blots of wildtype (KT3082) (C), *MAPKK$^{byr1.DD}$* (KT3435) (E) and *ras1.G17V* (KT3084) (G) cells. Three biological replicates were used for quantitation (error bars are ±SEM). α-tubulin was used as a loading control and quantitation was carried out using the Image Studio ver2.1 software (Licor Odyssey CLx Scanner). For the wildtype samples in (C), the % of cells mating is also indicated. The wildtype **pp**MAPK^{Spk1} result (C) is also presented in (E) and (G) as a reference. (D), (F) and (H) Cellular morphology (brightfield) and localization of MAPK^{Spk1}-GFP over a 24 hour time-course in wildtype (D), *MAPKK$^{byr1.DD}$* (F) and *ras1.G17V* (H) cells. Time after induction of mating in hours is indicated on the left. At each time point, a bright-field image and a GFP signal image were taken and processed as described in materials and methods. Green asterisks in the time 24 h in the ras1.G17V cell image (H) indicate auto-fluorescence signal from inviable cell debris, which were presumably produced through cytokinesis failure or cell lysis. Yellow arrows in panels (D) and (F) indicate transient accumulation of MAPK^{Spk1}-GFP at the shmoo tips. Scale bars represent 10μm.

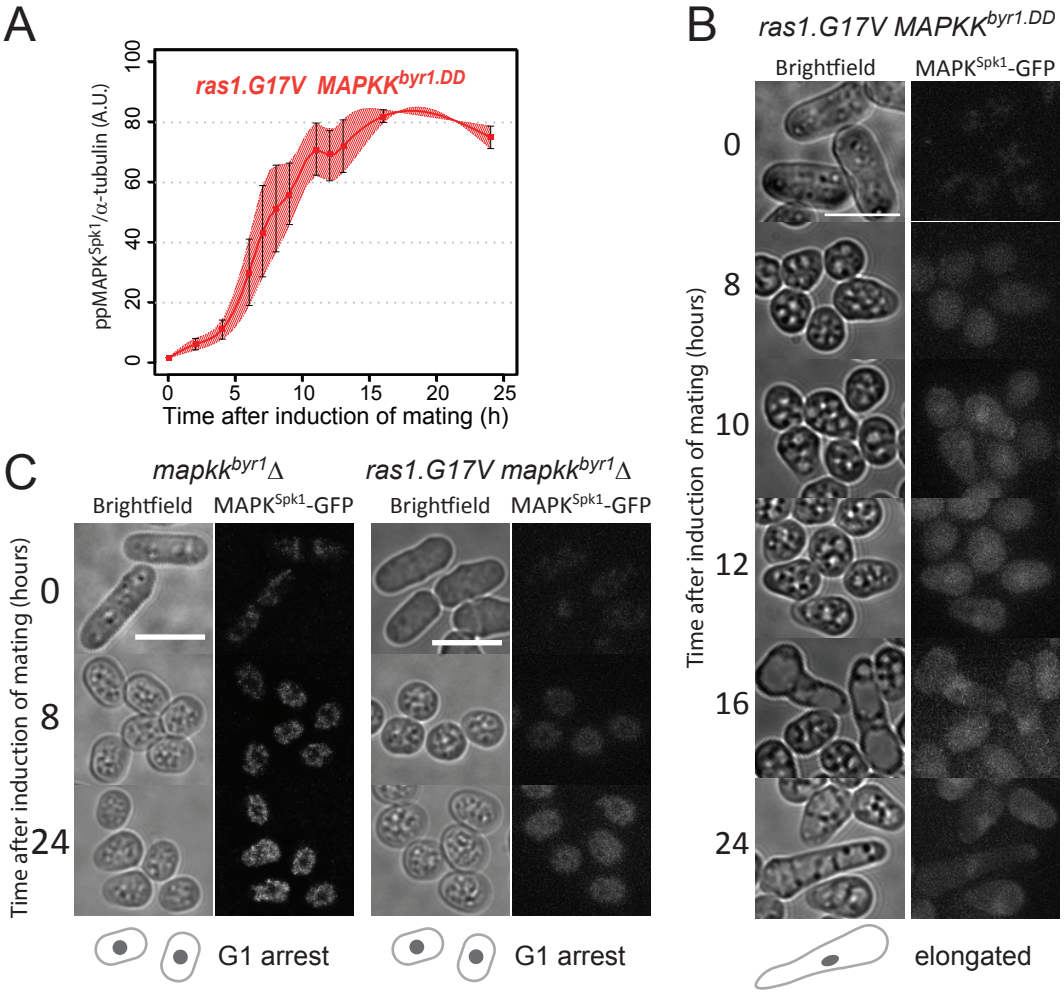

Figure 2. In the *ras1.G17V MAPKK*$^{byr1.DD}$ double mutant, the MAPK^{Spk1} phosphorylation profile follows *MAPKK*$^{byr1.DD}$ single mutant phenotype whilst cell morphology mimics the *ras1.G17V* single mutant phenotype.

(A) MAPK^{Spk1} phosphorylation status in the *ras1.G17V MAPKK*$^{byr1.DD}$ double mutant cells (KT3439). Cells were induced for mating by the plate mating assay system as described in the materials and methods. Quantitated **pp**MAPK^{Spk1} signal (arbitrary unit) from western blots is presented. Results of two biological replicates (each derived from three technical replicates, error bars are ±SEM) are presented in red. (B) The terminal mating phenotype of *ras1.G17V MAPKK*$^{byr1.DD}$ double mutant is a phenocopy of *ras1.G17V* single mutant which shows the "elongated" morphology. Images were taken of *ras1.G17V MAPKK*$^{byr1.DD}$ double mutant (KT3439) in the same way as in Fig. 1. Time after induction of mating in hours is indicated on the left. (C) There is no morphological change in the absence of MAPK^{Spk1} signalling. Cell images of *MAPKK*^{byr1}*Δ* (KT4700) and *ras1.G17V MAPKK*$^{byr1.DD}$ (KT5030) strains are shown. Images were taken in the same way as in Fig. 1. Time after induction of mating in hours is indicated on the left of each series. Scale bars represent 10μm.

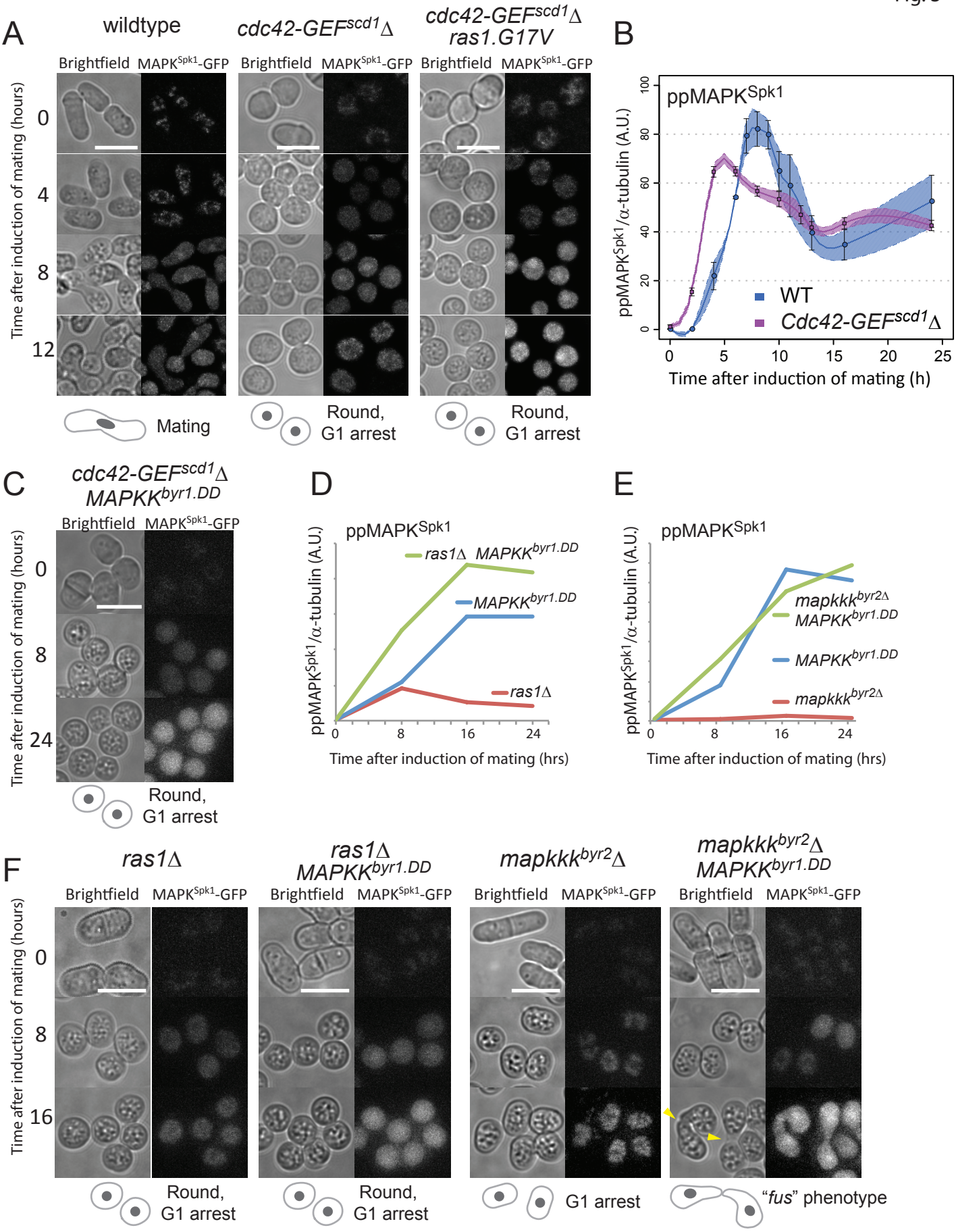

Figure 3. Ras1 activates both MAPK^{Spk1} and Cdc42 pathways during pheromone signalling.
(A) *scd1Δ* morphology and MAPK^{Spk1}-GFP signal. Images of WT (KT3082), *scd1Δ* (KT4061) and *scd1Δ ras1.G17V* double mutant (KT4056) were taken in the same way as in Fig.1. Numbers on the left represents hours after induction of mating. (B) MAPK^{Spk1} phosphorylation state in *scd1Δ* (KT4061) cells after mating induction. Results of three biological replicates (error bars are ±SEM) are presented. The wildtype result presented in Fig.1 (C) is also shown in blue as a reference. (C) Cell images of *scd1Δ MAPKK$^{byr1.DD}$* double mutant (KT4047) were taken in the same way as in Fig.1. Numbers on the left represents hours after induction of mating. (D) MAPK^{Spk1} phosphorylation state in *ras1Δ* (KT4323), *MAPKK$^{byr1.DD}$* (KT3435) and *scd1Δ MAPKK$^{byr1.DD}$* (KT4359) cell extracts. Original Western blotting data is presented in Fig. S3A. (E) MAPK^{Spk1} phosphorylation state in *mapkkk^{byr2}Δ* (KT3763), *MAPKK$^{byr1.DD}$* (KT3435) and *mapkkk^{byr2}Δ MAPKK$^{byr1.DD}$* (KT4010) cell extracts. Original Western blotting data is presented in Fig. S3B. For (D) and (E), quantification was carried out using the Image Studio ver2.1 (Li-cor). (F) Cell images of the strains mentioned in (D) and (E) were taken in the same way as in Fig.1. Numbers on the left represents hours after induction of mating. For all the images presented in (A), (C) and (F), scale bars represent 10μm.

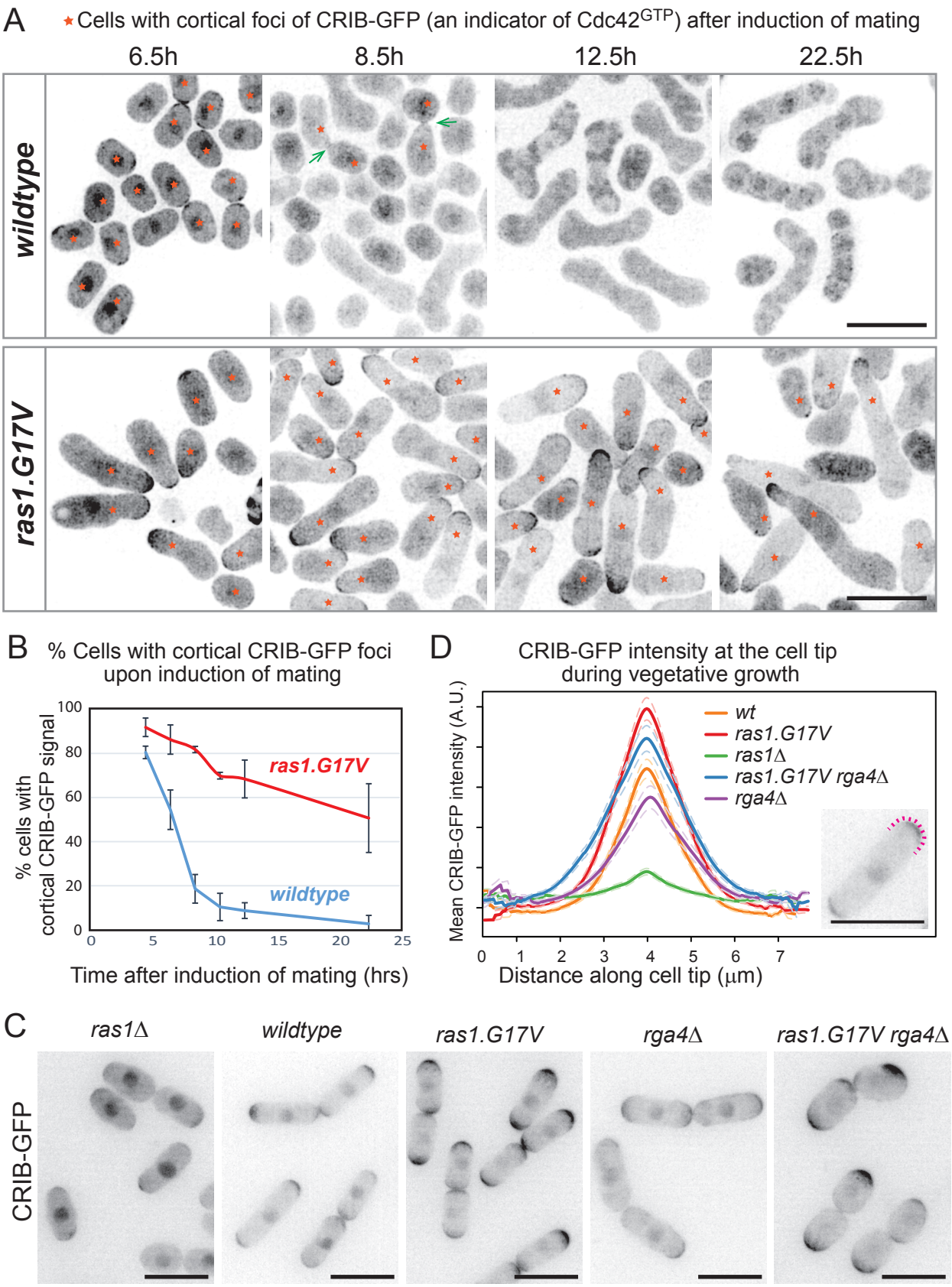

Figure 4. Ras1.G17V induces cortical Cdc42^{GTP} accumulation
(A) Cell morphology and localisation of Cdc42^{GTP}, indicated by CRIB-GFP signal, during the sexual differentiation process. Wildtype (KT5077) and *ras1.G17V* (KT5082) mutant cells were induced for sexual differentiation by the plate mating assay condition (Materials and Methods) and live cell images were taken at the indicated time after induction of mating/sexual differentiation. Representative CRIB-GFP signal images are presented. Cells with cortical CRIB-GFP foci are indicated by orange stars. Rapidly-disappearing CRIB-GFP signals at the fusion site of wildtype mating cells are indicated by green arrows at time 8.5h image. Scale bar: 10 μm. (B) Quantitation of the results presented in (A). At each time point (4.5h, 6.5h, 10.5h, 12.5h and 22.5h after induction of mating/sexual differentiation), 150 cells were examined whether they have cortical CRIB-GFP foci. % cells with cortical CRIB-GFP foci is presented. The experiment was repeated for three times and the mean values and SDs are plotted in the graph. (C) Cell morphology and localisation of Cdc42^{GTP}, indicated by CRIB-GFP signal, during vegetative growth. Representative CRIB-GFP signal images of cells of wildtype (KT5077), *ras1Δ* (5107), *ras1.G17V* (KT5082), *rga4Δ* (5551) and *rga4Δ ras1.G17V* (KT5554) are presented. Scale bar: 10 μm. (D) Quantitated CRIB-GFP signals on the cell cortex of cells presented in (C). Intensity of GFP signal on the cell cortex was measured along one of the cell tips as indicated as a magenta dotted line in the example image on the right (Scale bar: 10 μm) as stated in the Materials and Methods. 40 cells without septum were measured for each strain and the average curve from all aligned traces per strain was calculated, and displayed with respective standard error of the mean curves (dashed lines) as described in Materials and Methods.

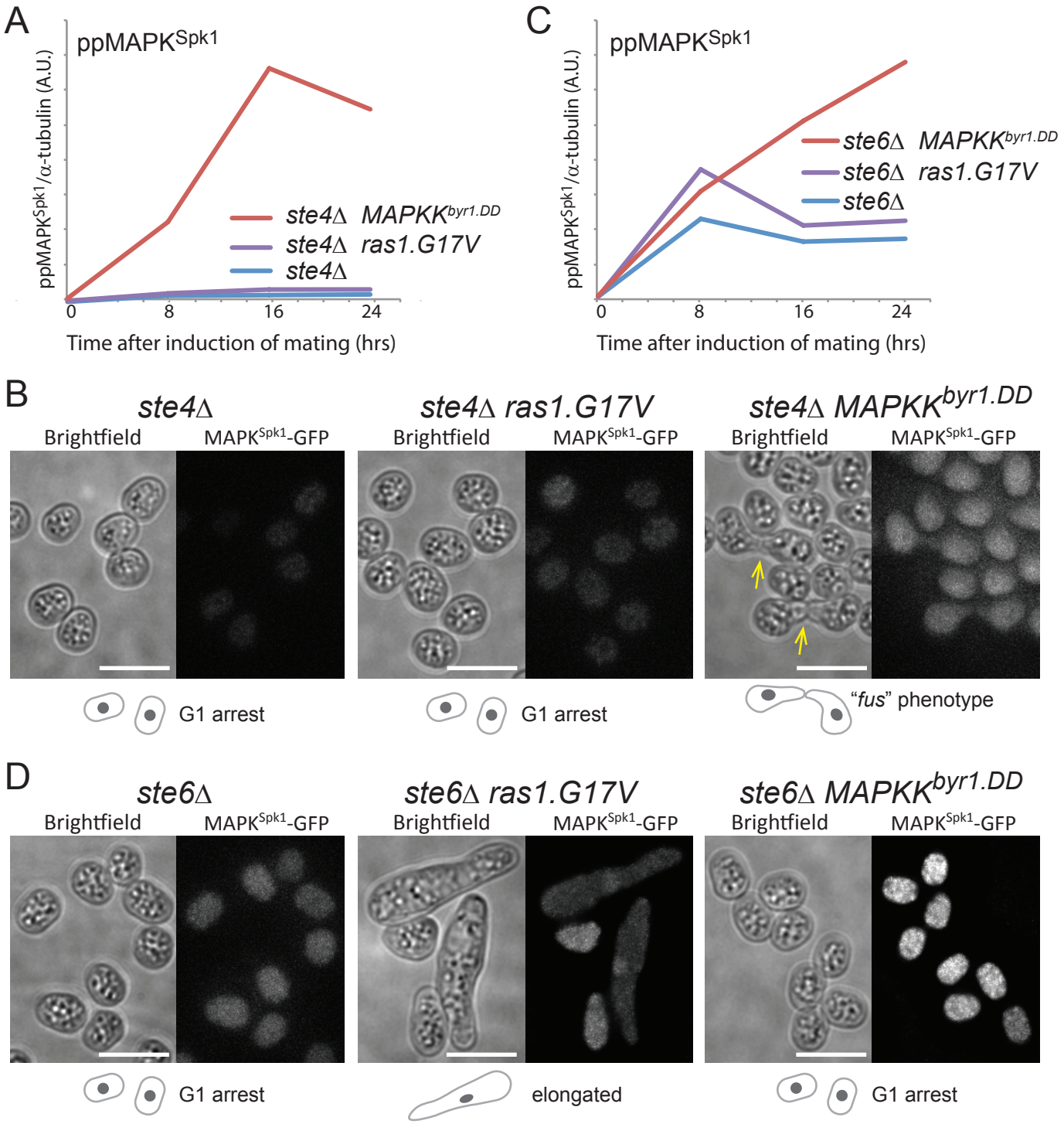

Fig. 5. Distinct contributions of Ste4 and Ste6 to MAPK^{Spk1} phosphorylation.
(A) Ste4 is essential for MAPK^{Spk1} activation. MAPK^{Spk1} phosphorylation status in *ste4Δ* (KT4376), *ste4Δ ras1.G17V* (KT5143) and *ste4Δ MAPKK$^{byr1.DD}$* (KT5136) at times-points 0, 8 ,16 and 24 hours post mating induction are presented. Original Western blotting membranes are presented in Fig. S3C. (B) Incapability of *ste4Δ* to cause pheromone-induced morphological change is suppressed by *MAPKK$^{byr1.DD}$* but not by *ras1.G17V*. Cell images of *ste4Δ* (KT4376), *ste4Δ ras1.G17V* (KT5143) and *ste4Δ MAPKK$^{byr1.DD}$* (KT5136) strains were taken 24 hours after induction of mating. Scale bar: 10 μm. (C) Lack of Ste6 does not result in the complete loss of MAPK^{Spk1} phosphorylation. MAPK^{Spk1} phosphorylation status in *ste6Δ* (KT4333), *ste6Δ ras1.G17V* (KT4998) and *ste6Δ MAPKK$^{byr1.DD}$* (KT5139) at times-points 0, 8 ,16 and 24 hours post mating induction are presented. Original Western blotting membranes are presented in Fig. S3D. (D) Incapability of *ste6Δ* to cause pheromone-induced morphological change is suppressed by *ras1.G17V* mutation but not by *MAPKK$^{byr1.DD}$* mutation. Cell images of *ste6Δ* (KT4333), *ste6Δ ras1.G17V* (KT4998) and *ste6Δ MAPKK$^{byr1.DD}$* (KT5139) strains were taken 24 hours after induction of mating. Scale bar: 10 μm.

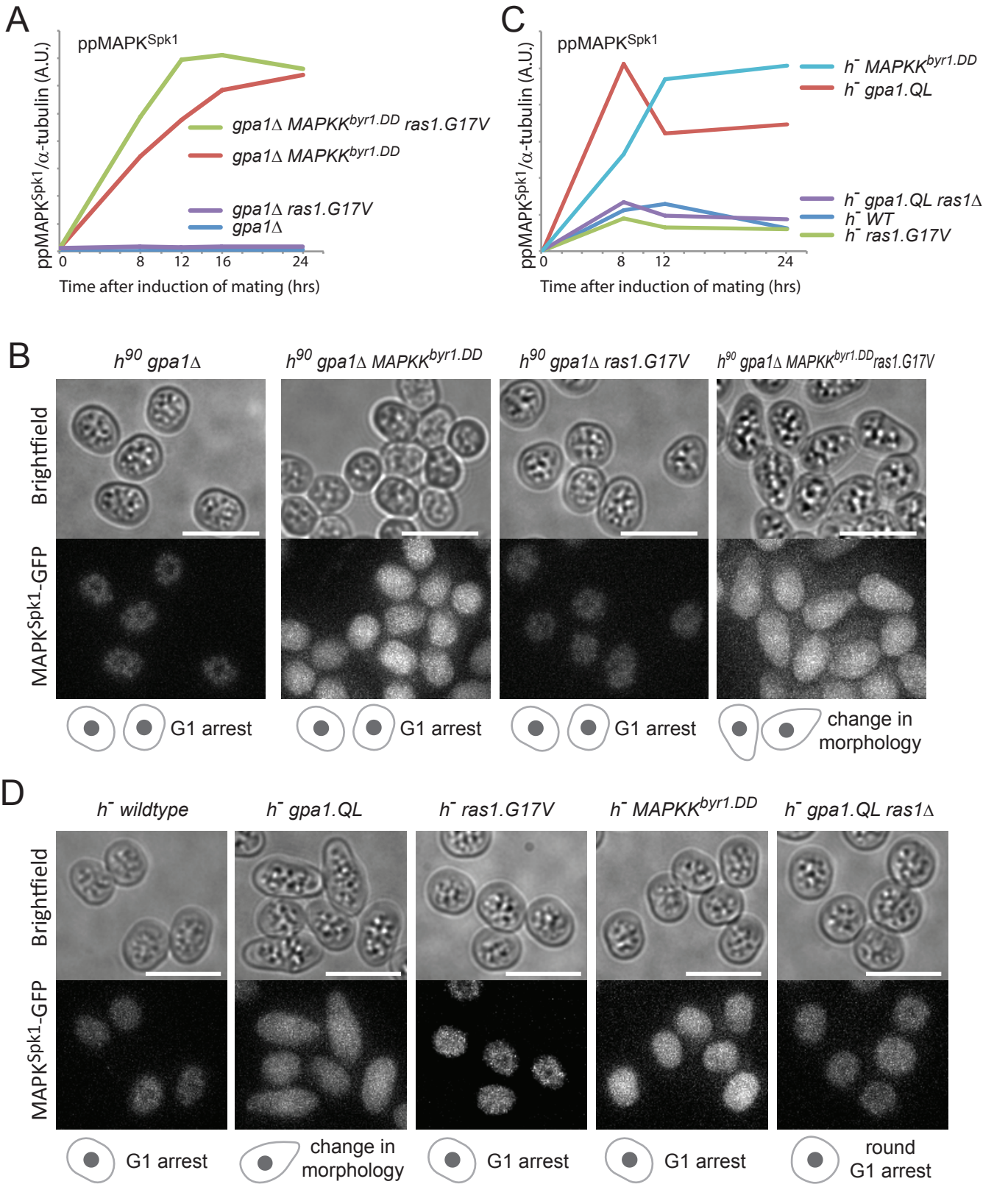

Fig. 6. Gpa1 transduces the pheromone signalling by activating MAPK^{Spk1} and Ras1 pathways.
(A) MAPK^{Spk1} phosphorylation status in homothallic *gpa1Δ* (KT4335), *gpa1Δ ras1.G17V* (KT5023), *gpa1Δ MAPKK$^{byr1.DD}$* (KT4353) and *gpa1Δ ras1.val17 MAPKK$^{byr1.DD}$* (KT5035) at times-points 0, 8 ,12, 16 and 24 hours after mating induction. Original Western membrane is presented in Fig. S4A. (B) Cell images of the above mentioned strains at 16 hours after mating induction. All the cell images were taken and processed as in Figure 1. Scale bar is 10 µm. (C) MAPK^{Spk1} phosphorylation status in *h⁻* WT (KT4190), *h⁻ gpa1.QL* (KT5059), *h⁻ ras1.G17V* (KT4233), *h⁻ gpa1.QL ras1Δ* (KT5070) and *h⁻ MAPKK$^{byr1.DD}$* (KT4194) at times-points 0, 8 ,12 and 24 after mating induction. Note that while the activation induced in the gpa1.QL mutant was down-regulated, *MAPKK$^{byr1.DD}$* induced a constitutive activation. Original Western membrane is presented in Fig. S4B. (D) Cell images of the above strains at 12 h after induction of mating. All the cell images were taken and processed as in Figure 1. Scale bar is 10 µm.

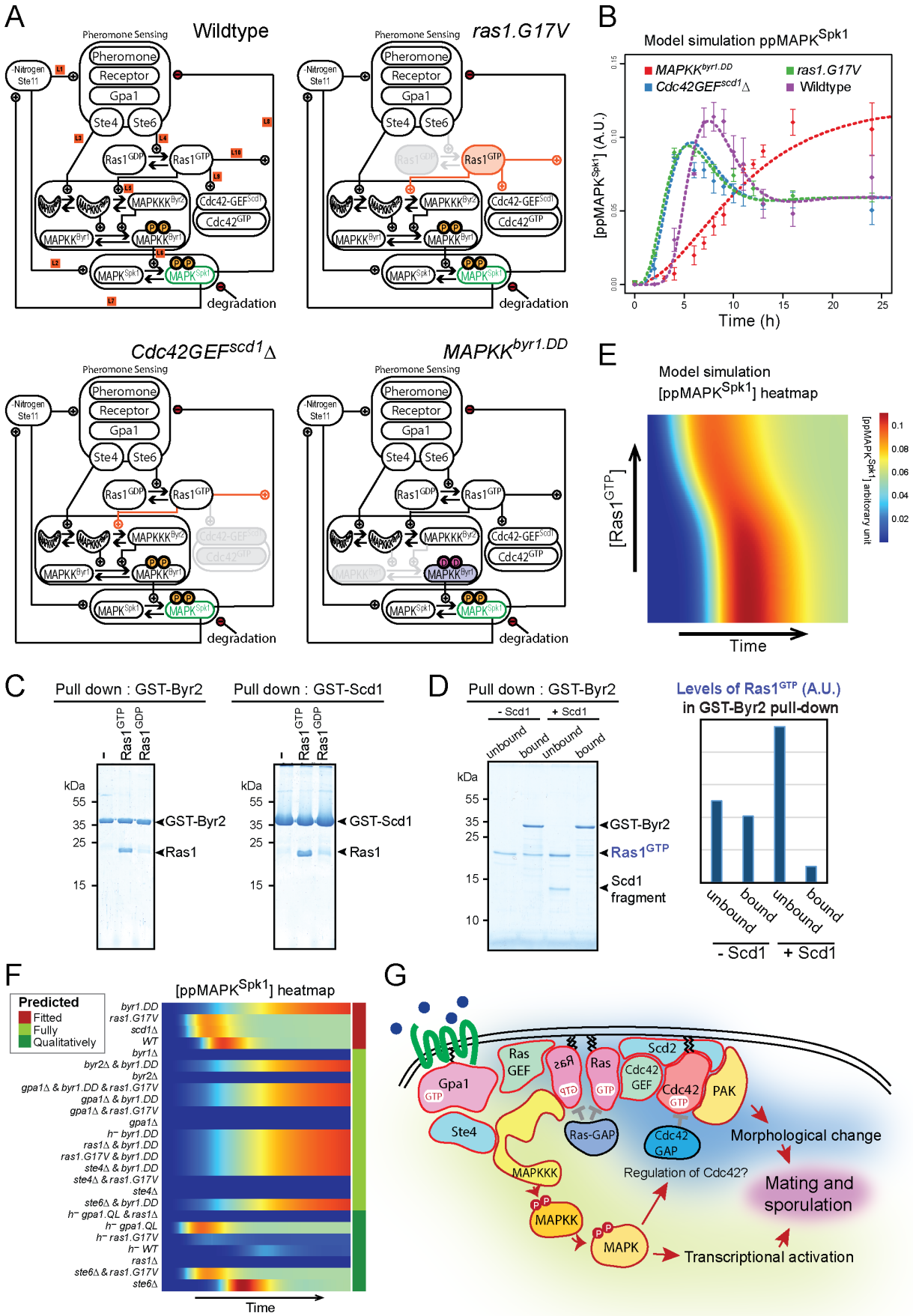

Fig. 7. Mathematical modelling of the fission yeast pheromone pathway dynamics.
(A) Components and frameworks of the mathematical model in wildtype and signalling mutants: *ras1.G17V, Cdc42GEF^{scd1}Δ*, and *MAPKK$^{byr1.DD}$*. Changes corresponding to each mutant are indicated as follows: Grey: removed components or interactions, orange: increased level of activity. For the exact implementation of the mutants, see Materials and Method. The measured component, **pp**MAPK^{Spk1}, is highlighted in green. (B) Measured and simulated **pp**MAPK^{Spk1} activation profiles in wildtype, *ras1.G17V, Cdc42GEF^{scd1}Δ* and *MAPKK$^{byr1.DD}$* mutants. Dashed lines: model simulations. Diamonds: experimental data presented in Fig. 1C, E, G, and Fig. 3B; error bars: SEM. (C) GTP-loaded Ras1.G17V (1-172) directly binds to Byr2 (65-180) and Scd1 (760-872). *In vitro* GST pull-down assays of bacterially expressed Ras1.G17V (1-172), GST-Byr2 (65-180) and GST-Scd1 (760-872) were conducted as described in materials and methods. GTP-loaded Ras1.G17V (1-172) was found to bind to both GST-Byr2 (65-180) and GST-Scd1 (760-872). (D) Two Ras1 effectors, Byr2 and Scd1, compete for GTP-loaded Ras1.G17V (1-172). *In vitro* GST pull-down assays of bacterially expressed Ras1.G17V (1-172) and GST-Byr2 (65-180) were conducted as in (A). Addition of Scd1 (760-872) fragment interfered with Ras1-Byr2 binding (the 4th lane). Quantitated signal

intensities of the Ras1.G17V (1-172) band in the gel are shown in the right panel. (E) Simulated ppMAPK^{Spk1} dynamics in the wildtype model at increasing concentrations of Ras1^{GTP} added *in silico* to the system. Increased Ras1^{GTP} concentration causes advanced and reduced **pp**MAPK^{Spk1} peak intensities. (F) The model fitted to the 4 strains (as above, in red) correctly predicts ppMAPK^{Spk1} dynamics in the additional 21 signalling mutant strains measured in this study.(G) Schematic diagram of the fission yeast pheromone signalling pathway, highlighting the branched pheromone sensing, and that ultimately both branches are necessary for mating.